Daniel Harper
Lars Maukon Muren

Active Damping of Bridge Section Models

Master's thesis in Mechanical Engineering
Supervisor: Gunnstein Thomas Frøseth
December 2019

Master's thesis

NTNU
Norwegian University of Science and Technology
Faculty of Engineering
Department of Structural Engineering

NTNU
Norwegian University of
Science and Technology

Daniel Harper
Lars Maukon Muren

Active Damping of Bridge Section Models

Master's thesis in Mechanical Engineering
Supervisor: Gunnstein Thomas Frøseth
December 2019

Norwegian University of Science and Technology
Faculty of Engineering
Department of Structural Engineering

NTNU
Norwegian University of
Science and Technology

This is the thesis of Daniel Harper and Lars Maukon Muren for their MSc degree in Mechanical Engineering at NTNU, 2019. The project was carried out for the Department of Structural Engineering.

We would first of all like to thank our supervisor Gunnstein Thomas Frøseth for helping us out with everything from structural dynamics theory to guidance on how to write the report. We both appreciate the consultancy he provided while working on this project and are proud to be the first students writing a master thesis under his guidance. We would also like to thank Steinar Seehuus, Bjørn Stickert Schjølberg and the rest of the guys at the Structural Engineering Laboratory for assistance and guidance. This project would not have been possible without their help. We would finally like to thank Bartosz Siedziako for letting us use figures from his PhD thesis.
Daniel Harper and Lars Maukon Muren, Oslo, December 27, 2019

First, I want to thank Lars Maukon Muren for the work he has done in this project, writing this thesis together has been a true pleasure and I am very grateful for having had that opportunity. I also want to thank NTNU for creating a great environment for learning and socialising with other students, I have met many of my best friends at this university. I want to thank Tomas Norgård Gabrielsen for suggesting engineering as my choice of study. This suggestion is what led me into the field of science and technology and I now believe this was the best choice I could have made. I also want to thank my girlfriend Ingvild Areng, for always standing by my side and supporting me while writing this thesis.
Daniel Harper, Oslo, December 22, 2019

Thanks to Daniel for always staying positive and helpful in difficult times - both in this project and as a friend. Thanks to my classmates which have contributed to five exciting years in Trondheim, both academically and socially. Thanks to my two grandfathers who have stayed supportive and helped me out in different tasks for as long as I can remember. I could not have asked for better technical and scientific role models.
Lars Maukon Muren, Asker, December 22, 2019

Abstract

When performing wind tunnel experiments on bridge section models in the Fluid Mechanics Laboratory at NTNU, unwanted high frequent vibrations may occur in the models, due to wind and motion induced forces. This thesis discusses different actuators, sensors and control algorithms for developing an active damping solution for reducing these high frequent vibrations. This was done by carrying out experiments on an aluminum test beam and develop a MATLAB simulation program for further testing. Both the experimental and numerical results suggest that solenoids are well suited for vibration reduction in systems subjected to motions caused by an initial displacement. However, for experiments with random induced forces - which are more relevant to the wind tunnel case - voice coil actuators perform better than solenoids, based on simulations with the developed MATLAB program. Further experimental testing with voice coil actuators are necessary to optimize the application. A suggestion to how this can be done is included, with the use of a CompactRIO, an accelerometer, a servo drive and a voice coil actuator.

Contents

Nomenclature

Abbreviations

AMD	Active mass damper
DOF	Degree of freedom
DVF	Direct velocity feedback
$FIFO$	First-in first-out
$FPGA$	Field programmable gate array
FFT	Fast fourier transform
LNF	Linear negative feedback
$MDOF$	Multi degree of freedom
N/A	Not available
$SDOF$	Single degree of freedom
TMD	Tuned mass damper
VCA	Voice coil actuator
VDT	Velocity-displacement threshold
VT	Velocity threshold

Symbols

A	Amplitude [m]
A_r	Area [m^2]
B	Magnetic flux density [Wb]
$\mathbf{C}$	Damping matrix
c	Damping coefficient [Ns/m]
c_{cr}	Critical damping coefficient [Ns/m]
D	Dynamic amplification factor
E	Energy [J]
F	Force [N]
f	Natural frequency [Hz]
g	Gravitational acceleration [$9.81m/s^2$]

I	Current $[A]$
I_y	2nd moment of inertia $[m^4]$
$\mathbf{K}$	Stiffness matrix
k	Stiffness $[N/m]$
L	Length $[m]$
$\mathbf{M}$	Mass matrix
m	Mass $[kg]$
N	Number of, quantity
n_{DOF}	Number of degrees of freedom
$\mathbf{P}(\mathbf{t})$	External load vector
$p(t)$	External force varying with time $[N]$
T	Kinetic energy $[J]$
t	Time $[s]$
U	Potential energy $[J]$
u	Displacement $[m]$
$\dot{u}$	Velocity $[m/s]$
$\ddot{u}$	Acceleration $[m/s^2]$
V	Voltage $[V]$
v	Velocity $[m/s]$
β	Frequency ratio, ω/ω_1
β_{nb}	Constant in Newmark-beta method
γ	Product of damping ratio and natural frequency, $\xi\omega_n$
γ_{nb}	Constant in Newmark-beta method
δ	Logarithmic decrement
μ	Mass ratio in 2-DOF system, m_2/m_1
ξ	Damping ratio
ρ	Density $[kg/m^3]$
ϕ	Phase angle
ω_n	Natural frequency $[rad/s]$
ω_D	Damped natural frequency $[rad/s]$

Chapter 1

Introduction

In order to secure that engineering applications operate as intended, it is important to be familiar with the theory of mechanical vibrations. This covers a wide range of fields, from vibration in precision tools to swaying of large buildings and bridges [18]. There are numerous reasons to control the motion of structures, the most important being to prevent failure in constructions, that may be dangerous to humans. This can occur due to fatigue fractures, fractures caused by large strains in transient events (e.g strong wind gusts) or fracture as a consequence of general system instability (e.g. fluttering) [18]. Securing the comfort of people is also important. This concerns everything from reducing swaying of skyscrapers to bike suspensions. At a smaller scale, precision applications, such as metal machining tools, may not function optimally when exposed to large vibrations [11]. Many of these problems may be addressed by introducing vibration reduction. In general, this can be obtained through three main topics: stiffening, isolation and damping [18]. By making constructions stiffer, one shifts the natural frequencies to higher values with less energy (Equation 2.2). By isolation, one prevents vibrations in critical sections of the construction. By damping, one dissipates the vibration energy, and thus reduces the vibrating amplitude [18]. This master thesis will mainly discuss damping as the method of vibration reduction. *Passive* and *active* are the two main methods of damping [18]. In passive damping, one construct the application to damp out the motion of pre-calculated frequencies. This may be achieved through material selection or dissipating the energy to an additional construction part, for example a tuned mass damper (TMD) [18]. The main disadvantage of passive damping methods is that only a defined range of frequencies can be addressed. This works for constructions with well known and determinable dynamic properties, but may be a problem for applications with varying properties under varying conditions. Active damping is another approach which uses sensors, actuators and a regulator with a control algorithm to reduce the response magnitude. The concept is depicted in Figure 1.1. The sensors may provide data for strain, force, velocity, acceleration or another physical measurement, while the actuators provide a force or another response to the structure through the control algorithm [18].

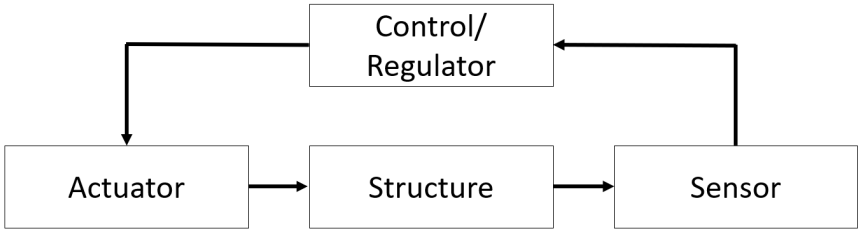

Figure 1.1: Concept of active damping.

Dynamic behaviour of bridges is an important research field in modern society, where longer and slender bridges are built in more and more extreme environments. This concerns both railway bridges, floating bridges, submerged tube bridges as well as long span suspension bridges. The Department of Structural Engineering at NTNU is currently monitoring several bridges on the west coast of Norway and is heavily involved in important research on the project "Ferjefri E39" between Trondheim and Kristiansand [3]. The goal of this project is to substitute the use of ferries with different bridge concepts to cross the numerous fjords on the existing road. As a part of the research on wind induced mechanical vibrations on bridges, NTNU's largest wind tunnel at the Fluid Mechanics Laboratory is frequently used. This tunnel has a $2x3m$ section and can provide a maximum wind velocity of $100km/h$ [3]. Figure 1.2 shows a bridge deck model mounted in the wind tunnel.

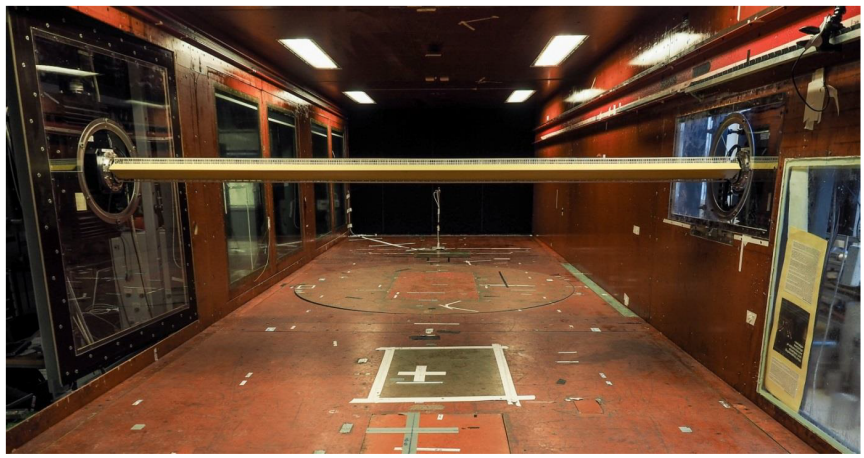

Figure 1.2: Bridge girder section model mounted for experiments in the largest wind tunnel of the Fluid Mechanics Laboratory of NTNU [19].

Experiments are important to obtain data on how mean wind, turbulence and vortex shedding affect the behaviour of suspension bridges. The bridge decks for testing are typically milled in gurit material around an aluminum pipe, to make it both stiff and light [20]. Figure 1.3 illustrates a section model construction, more specifically the model of the Hardanger Bridge deck.

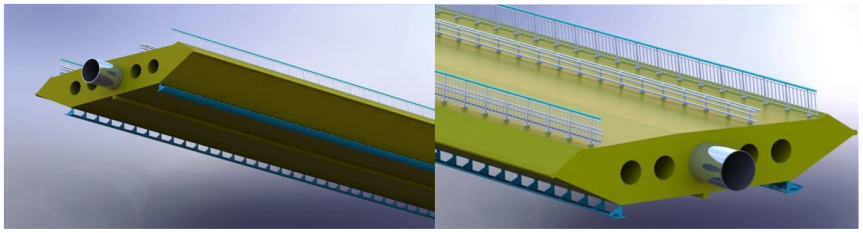

Figure 1.3: Modelling of Hardanger Bridge girder section model [19].

The models presented here are section models, which often are more convenient than full bridge models when it comes to experiments, due to the possibility of testing in reasonably sized wind tunnels [20]. This means that the test itself can be performed at a larger scale [20]. To obtain aerodynamic properties of the bridge, one can perform tests in either free or forced vibration. Figure 1.4 shows the forced vibration rig developed for wind tunnel experiments at NTNU.

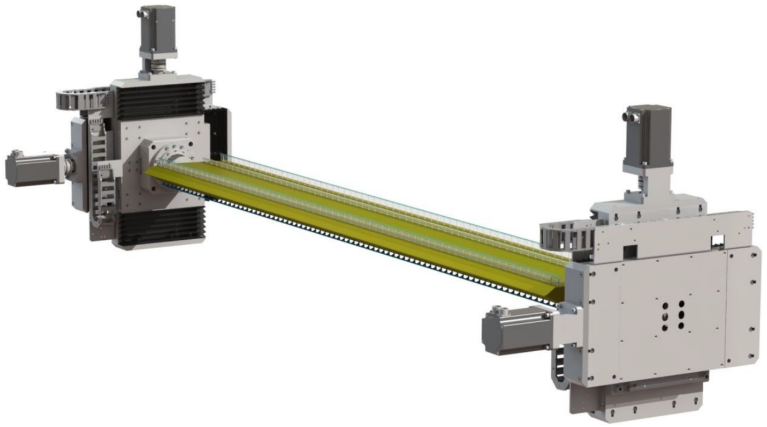

Figure 1.4: The forced vibration rig developed at NTNU [19].

This rig has the ability to induce motions in vertical and horizontal direction, as well as the rotational direction of the pitching moment [20]. The rig may also measure the forces due to wind in the same directions. The idea is to simulate real bridge section movements and measure the above mentioned forces as a part of estimating the aerodynamic properties [20]. However, the bridge section motion is not always fully controlled by the actuators of the vibration rig. Unwanted high frequency vibrations may occur in the model, due to the small scale section in a strong wind velocity field. These vibrations does not represent a full scale dynamic effect. It is therefore desirable to test if the use of an active damping application may reduce these high frequency vibrations, enabling more accurate tests in the wind tunnel. This project will present active damping theory and perform tests on a simple aluminum test rig to explore the use of actuators, algorithms and sensors to perform this task.

Chapter 2

Theory

2.1 Single Degree of Freedom System

In order to be familiar with the dynamic properties of the bridge models, some general theory on structural dynamics need to be stated. Dynamic amplification may occur if the frequency of the load gets close to one of the natural frequencies of the system. This could lead the construction to deformation or failure due to increasing amplitude in the response. The natural frequency of a system is the frequency a system tends to take in the absence of any external forces [5], after first being set to motion. A system will always have equal numbers of DOFs and natural frequencies. This means that the SDOF system of Figure 2.1 will have one single natural frequency.

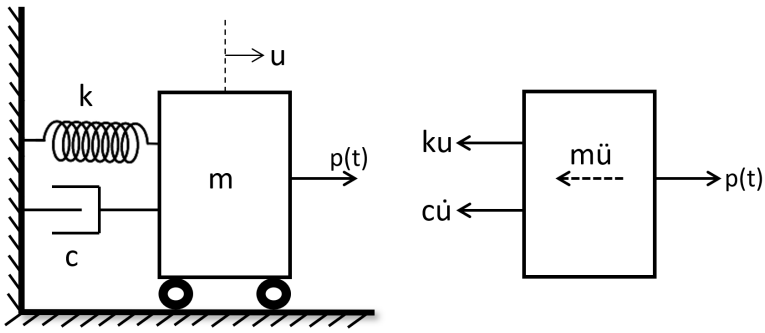

Figure 2.1: SDOF system on a friction-free surface with damping and stiffness.

By studying the free body diagram of Figure 2.1, it is possible to establish the equation of motion for a SDOF system as

$$m\ddot{u} + c\dot{u} + ku = p(t), \tag{2.1}$$

where m is the mass, c is the damping coefficient, k is the spring stiffness, $p(t)$ is an

external force, and u is the displacement with its derivatives. If the damping is set to zero, the natural frequency is given by

$$\omega_n = \sqrt{\frac{k}{m}}, \tag{2.2}$$

and are dependent on mass and stiffness.

2.2 Damping Theory

In reality, all dynamic systems contain damping due to dissipation of energy, for example in the form of heat. It is convenient to introduce the damping ratio, ξ, as

$$\xi = \frac{c}{c_{cr}}, \tag{2.3}$$

where c_{cr} is the critical damping defined as

$$c_{cr} = 2\sqrt{km}. \tag{2.4}$$

The damping ratio tells immediately if the system is underdamped ($\xi < 1$), critically damped ($\xi = 1$) or overdamped ($\xi > 1$) [21]. The meaning of this is illustrated in Figure 2.2, where the responses of a SDOF system with an initial displacement is presented for the three different cases of damping.

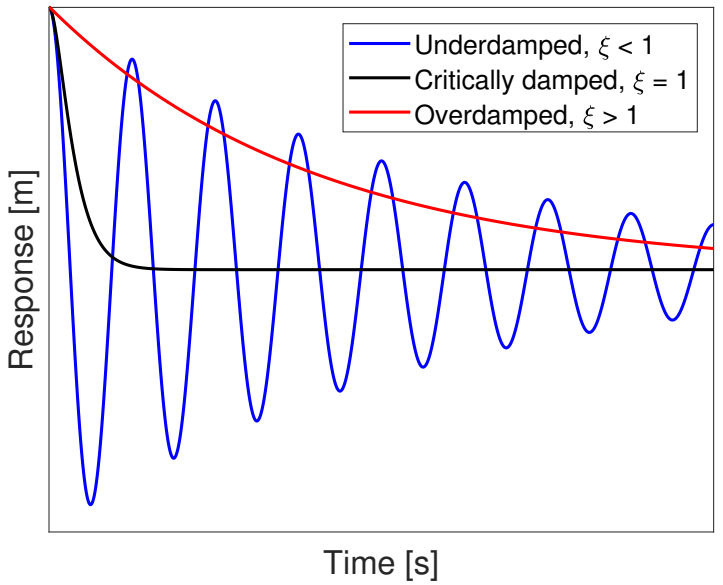

Figure 2.2: Response of underdamped, critically damped and overdamped systems.

Underdamped systems will oscillate around a state of equilibrium, while overdamped systems never will reach the point of zero displacement due to high damping and dissipation of energy. The critically damped case represent the state where the system will reach the state of equilibrium with no oscillations. The systems studied in this thesis are underdamped systems with a low damping ratio. The damped natural frequency, ω_D, is related to the natural frequency by

$$\omega_D = \omega_n \sqrt{1 - \xi^2}. \tag{2.5}$$

The damped natural frequency will then be approximately equal to the natural frequency for sufficiently low damping ratios. When measuring the response of a vibrating system, it is possible to derive the value of ξ. A system in free vibration with a given damping ratio will oscillate as

$$u(t) = A_0 e^{-\gamma t} sin(\omega_n t + \phi), \tag{2.6}$$

where $\gamma = \xi\omega_n$ [12], A_0 is the initial amplitude, t is time and ϕ is the phase angle. The exponential term $e^{-\gamma t}$ describes the decreasing amplitude due to damping in the system and $sin(\omega_n t + \phi)$ describes the oscillation. By performing a curve fit on the peaks in the data points of the response, one obtain the exponential coefficient γ. The natural frequency can easily be found through a Fourier Transform of the response, which yields the damping ratio $\xi = \gamma/\omega_n$. This curve fit is illustrated in Figure 2.3.

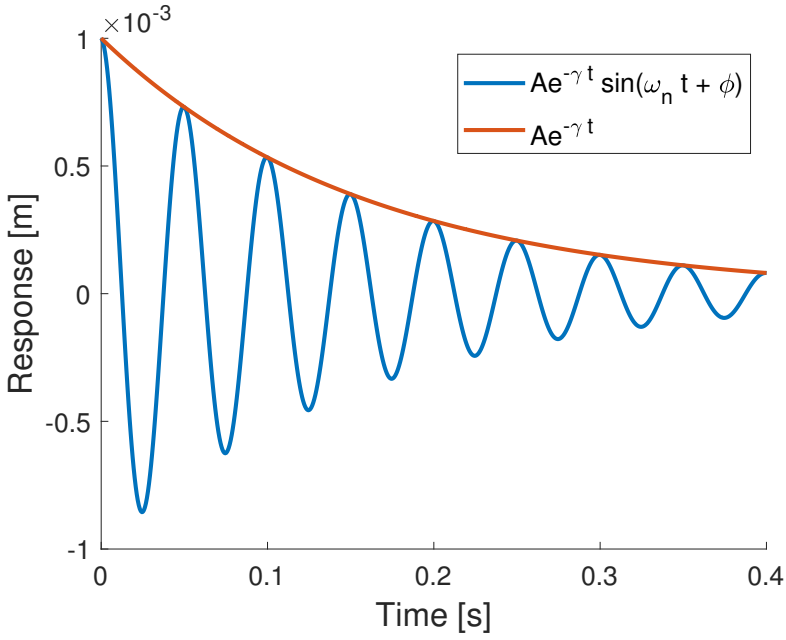

Figure 2.3: Illustration of envelope function of an underdamped system.

The damping ratio may also be obtained through measured response with the method of

logarithmic decrement. The logarithmic decrement, δ, is given by

$$\delta = ln(\frac{x_n}{x_{n+1}}), \tag{2.7}$$

where x_n and x_{n+1} are the values of two successive peaks of the signal. ξ is then given by [13]

$$\xi = \frac{1}{\sqrt{1 + (\frac{2\pi}{\delta})^2}}. \tag{2.8}$$

2.3 Multi Degree of Freedom System

Structures are often too complex to be modeled as SDOF systems. Thus it is necessary to expand the scalars of Equation 2.1 to matrices and a multi degree of freedom (MDOF) system. The motion may now be described as

$$\mathbf{M\ddot{u} + C\dot{u} + Ku = P(t)}, \tag{2.9}$$

where $\mathbf{K}$, $\mathbf{C}$ and $\mathbf{M}$ represent stiffness, damping and mass matrices, respectively. This yields a set of n_{DOF} equations of motion, where n_{DOF} represent the number of degrees of freedom. An example closely related to the tuned mass damper later investigated, is the 2-DOF spring-damper system of Figure 2.4.

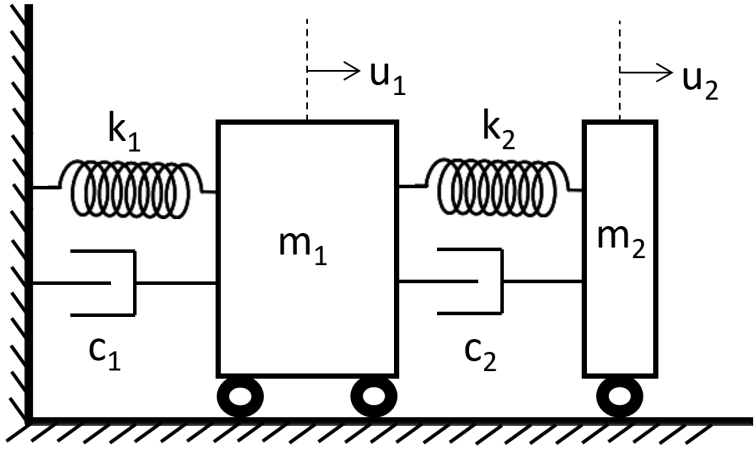

Figure 2.4: MDOF system on a friction-free surface with damping and stiffness.

The motions may now be described with matrices and Equation 2.9. For this particular example the equation of motion is

$$\begin{bmatrix} m_1 & 0 \\ 0 & m_2 \end{bmatrix} \begin{Bmatrix} \ddot{u_1} \\ \ddot{u_2} \end{Bmatrix} + \begin{bmatrix} c_1 + c_2 & -c_2 \\ -c_2 & c_2 \end{bmatrix} \begin{Bmatrix} \dot{u_1} \\ \dot{u_2} \end{Bmatrix} + \begin{bmatrix} k_1 + k_2 & -k_2 \\ -k_2 & k_2 \end{bmatrix} \begin{Bmatrix} u_1 \\ u_2 \end{Bmatrix} = \begin{Bmatrix} P_1(t) \\ P_2(t) \end{Bmatrix}. \tag{2.10}$$

2.4 Passive Damping with Tuned Mass Dampers

A classic approach to passively reduce the amplitude of vibrating structures is by utilizing a dynamic vibration absorber, also called tuned mass dampers (TMD). This is a simple system attached to the structure and contains a spring, damper and mass [7]. The idea is to determine properties of the TMD to reduce the vibrations of a certain frequency, so when that frequency is excited, the dynamic amplitude will reduce compared to the case with no TMD present [7]. Introducing TMDs to reduce the deformations may be a cheaper alternative than making the construction stiffer by increasing section area or change material. The formula for the natural frequency of a beam is given by [23]

$$f_n = \frac{K_n}{2\pi}\sqrt{\frac{EI_y}{A_r \rho L^4}}, \tag{2.11}$$

where f_n is the natural frequency in Hz, E is young's modulus, I_y is the second moment of inertia, L is the length of the beam, ρ is the density, and A_r is the area of the cross section. K_n is a constant dependent on beam boundary conditions and mode number. Multiplying the stiffness EI by 2 only increases the natural frequency with a factor of 1.4. Tuned mass dampers are today present in numerous well-known constructions, such as the Millennium Bridge in London [17] and in Taipei 101 Tower in form of the famous 660-tonne heavy pendulum [7]. Since TMD properties must be tuned to damp out one specific frequency, they are well suited for constructions where its natural frequencies and general motion is determinable and known. To further state important theory on tuned mass dampers, the simple MDOF system in Figure 2.4 is again studied, where the mass m_2 serve as the TMD. By applying a harmonic force of $p_0 cos(\omega t)$ to the structure, the equation of motion for the main system is given by

$$m_1\ddot{u_1} + (c_1 + c_2)\dot{u_1} - c_2\dot{u_2} + (k_1 + k_2)u_1 - k_2u_2 = p_0 cos(\omega t), \tag{2.12}$$

and the equation of motion for the TMD,

$$m_2\ddot{u_2} - c_2\dot{u_1} + c_2\dot{u_2} - k_2u_1 + k_2u_2 = 0. \tag{2.13}$$

This system can be solved to find the dynamic amplification factor of the primary mass. This factor is defined as

$$D_{u_1} = \frac{u_{1,max}}{u_{1,stat}}, \tag{2.14}$$

where the static response simply is given by the relation p_0/k_1. A reduced dynamic amplification factor means reduced response amplitudes and deformations. It can be shown that the dynamic amplification factor of the primary mass can be expressed as [24]

$$D_{u_1} = \sqrt{\frac{4\xi_2^2\beta^2 + (\beta^2 - \beta_e^2)^2}{4\xi_2^2\beta^2(\beta^2 - 1 + \mu\beta^2)^2[\mu\beta_e^2\beta^2 - (\beta^2 - 1)(\beta^2 - \beta_e^2)]^2}}, \tag{2.15}$$

where β is the ratio of loading frequency to natural frequency of primary system,

$$\beta = \frac{\omega}{\omega_1}, \tag{2.16}$$

β_e is the ratio of natural frequency of TMD to natural frequency of primary system,

$$\beta_e = \frac{\omega_2}{\omega_1}, \tag{2.17}$$

μ is the mass ratio between TMD and primary system,

$$\mu = \frac{m_2}{m_1}, \tag{2.18}$$

and ξ_2 is the damping ratio of the TMD,

$$\xi_2 = \frac{c_2}{2m_2\omega_2}. \tag{2.19}$$

The natural frequencies of the two components of the system are given by Equation 2.2. After choosing a mass ratio, it can be shown that the optimal values of β_e and ξ_2 to minimize D_{u_1} are given as [9]

$$\beta_{e,opt} = \frac{1}{1+\mu} \tag{2.20}$$

and

$$\xi_{2,opt} = \sqrt{\frac{3\mu}{8(1+\mu)^3}}. \tag{2.21}$$

2.5 Active Vibration Control

Passive damping systems are restricted to damp out frequencies within a limited range, and can not be directly modified or changed after installation [7]. Correct and reliable values of system properties and load are therefore of vital importance for the system to operate effectively. The use of Active Vibration Control (AVC) addresses the issues of passive damping by introducing the use of sensors and actuators to control the dynamic vibrations in structures [18]. This makes it possible to control a wider range of frequencies, which is convenient for systems with varying motions and dynamic properties. The key components of an AVC system is typically a sensor, controller and actuator [7]. The sensor determines the present state of the structure in terms of acceleration, velocity, displacement, force or other physical property [7]. The controller analyzes this data and computes actions needed to change the state of the structure, while the actuator performs these actions. *Connor & Laflamme* [7] give the following accurate definition of an AVC system: *"An active structural control system is one that has the ability to determine the present state of the structure, decide on a set of actions that will change this state to a more desirable one, and carry out these actions in a controlled manner and in a short period of time."* This definition introduces some important aspects in AVC. Accurate instrumentation is essential for determining the state of the structure correctly. This includes a known sensor sensitivity (for example between voltage signal and acceleration), as well as sufficient sampling frequency to be able to change the state in a short period of time. Reduction of

the delay time between a signal is read and analyzed, and a command is carried out, is also important. In AVC systems, the external force applied through the actuator could amplify vibrations instead of damping them, if the system is inaccurate or the control algorithm is mathematically incorrect [18].

2.5.1 Control Algorithms in Active Damping Vibration Control

The controller is the part of the AVC system that analyzes the input from sensors and decide on actions for the actuator to perform to reduce the dynamic vibrations of the system. A control algorithm is necessary. These algorithms are generally organized in two main categories, feedforward and feedback [7]. Feedforward algorithms use signals from a primary DOF to predict the necessary output in other DOFs, based on knowledge about the process and system [10]. This may apply to MDOF systems with coupled actuators and sensors. SDOF systems usually use a feedback algorithm, which unlike feedforward control is error based [10]. A classic approach is the Linear Negative Feedback (LNF) control, which determines actions of the actuators based directly on physical measurements, such as acceleration, velocity and displacement [7]. To investigate the effects LNF controls, the simple SDOF system of Figure 2.5 is studied.

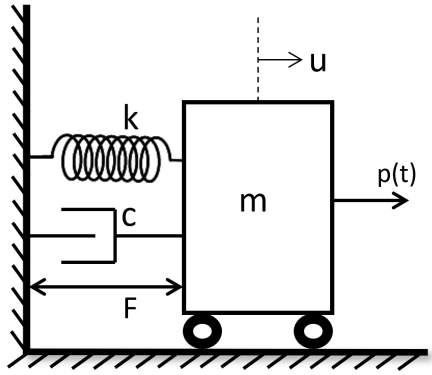

Figure 2.5: SDOF system exposed to external force (p) and internal force from actuator (F).

The mass is exposed to an external force p, as well as an internal force F from the actuator. This yields the equation of motion

$$m\ddot{u} + c\dot{u} + ku = F + p, \tag{2.22}$$

which may be rewritten with aid of Eq. 2.2, 2.3 and 2.4 as

$$\ddot{u} + 2\xi\omega\dot{u} + \omega^2 u = \frac{F}{m} + \frac{p}{m}. \tag{2.23}$$

F is now said to be a linear function of the acceleration, velocity and displacement of the structure,

$$F = -k_a\ddot{u} - k_v\dot{u} - k_d u \tag{2.24}$$

where k_a, k_v and k_d are constants free of choice, that could be optimized to the current application. This yields a new equation of motion

$$(1 + \frac{k_a}{m})\ddot{u} + (2\xi\omega + \frac{k_v}{m})\dot{u} + (\omega^2 + \frac{k_d}{m})u = \frac{p}{m}, \tag{2.25}$$

with equivalent fundamental frequency and damping ratio,

$$\omega_{LNF} = \sqrt{\frac{k + k_d}{m + k_a}} \tag{2.26}$$

and

$$\xi_{LNF} = \frac{1}{\omega_{eq}} \frac{c + k_v}{2(m + k_a)}, \tag{2.27}$$

respectively [7]. It is possible to draw important conclusions on the different negative feedback parameters through the equivalent dynamic properties above. Acceleration feedback will decrease both the fundamental frequency and damping ratio. Velocity feedback will increase the damping ratio, while displacement feedback will increase the fundamental frequency. Considering linear velocity feedback only is therefore a natural approach, and this is called Direct Velocity Feedback (DVF) control.

2.5.2 Actuators

The purpose of the actuator is to carry out action commands from the controller, based on the measured values of the sensor. An ideal actuator is able to apply a large force in a short period of time [7]. In general, one separates actuators in two main categories, *grounded* and *structure-borne* [18]. Grounded actuators apply forces on supports, while structure-borne actuators apply an internal force on the system [18]. The latter was used throughout this project. Many different engineering applications can be used with the purpose of applying forces to a system, for example hydraulic, electromechanical and electromagnetic applications [18]. Semi-active devices is also an option, which modifies the output forces by varying the dynamic properties of the actuator, meaning a constant energy input may induce a varying output force [7]. This may be done by varying stiffnesses, fluids and frictions in the device [7]. Piezoelectric actuators are another approach, which generates strain in a plane of the material when subjected to a voltage in the direction perpendicular to the plane. In this study, electromagnetic actuators were used, due to being reliable and commercially available [7]. Figure 2.6 shows the principle of a voice coil actuator (VCA) which operates as an electromagnetic transducer, converting electrical energy into mechanical energy by coils and a moving magnet.

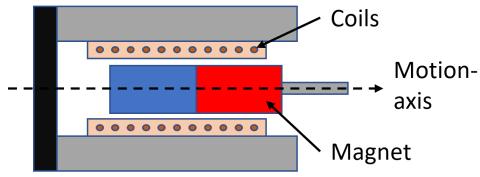

Figure 2.6: Schematic figure of voice coil actuator.

Lorentz' force principle states that the mechanical force on the moving part is given as [14]

$$F = kBLIN, \tag{2.28}$$

where k is a design constant, B is the magnetic flux density, I is the current, L is the length of the conductor and N is the number of conductors. This means that the input current of the actuator is proportional to the output force moving the piston. This force will by Newton's third law create a counter force on the structure the actuator is mounted on, and potentially damp out its motions. Changing the direction of the current will change the direction of the moving piston, and thus the direction of the counter force working on the structure. The induced voltage across the conductor is given as [14]

$$V = kBLvN, \tag{2.29}$$

where v is the velocity of the magnet. This means that the moving voice coil actuator will produce a force proportional to current and a voltage equally proportional to velocity of the conductor, implying that the VCA can be controlled by the amount of current and current direction [14]. Another possible approach is use of solenoids. A solenoid uses the same technology, but differs from a VCA by operating in an on-off manner. Figure 2.7 shows a solenoid, as well as a schematic drawing. The solenoids of Figure 2.7 are shown in off-state, that means that no current is sent through the coil.

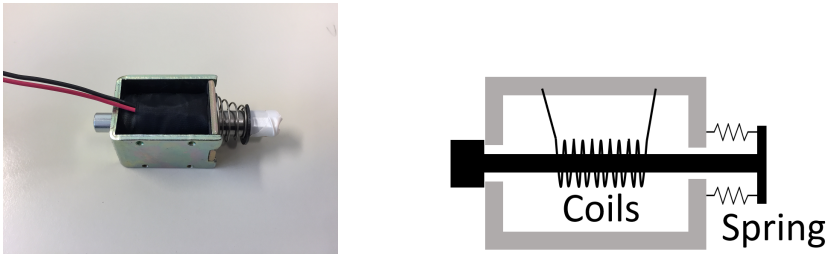

(a) Solenoid in off-state. **(b)** Schematic in off-state.

Figure 2.7: Concept of solenoids.

By applying a current to the coil, the piston will be pushed to tension the spring. By turning the current off, the stored forces of the springs will push the piston back to its off-state. This makes it possible to obtain forces in both directions from a solenoid, but at a predefined rate. Solenoids are cheap and an expedient alternative when making prototypes to test active damping applications. The power of a solenoid is often given as a plot of force as a function of stroke length. When the piston is fully placed inside the coil, the stroke is said to be zero. This is the case when the solenoid is turned on. In Figure 2.7, the solenoid is turned off, and the spring pushes the piston to its maximum range (in this case, 13 mm). In this particular state, the solenoid is said to be in a state of $13mm\ stroke$. In other words, $stroke$ is a measurement of where in the coil the piston is placed. Figure 3.1 shows an estimated force-stroke plot for a solenoid, based on datasheet specifications [1].

The plot shows that the solenoid is most efficient at low stroke, this means at the end of the process when turned from off to on. The efficiency is also dependent on the duty cycle, that is the ratio of on-time in a cycle, the lower duty cycle, the more power the solenoid may create.

2.5.3 Sensors and Signal Processing

The task of the sensor is to evaluate the state of the system, in order for the controller to give accurate action commands to the actuator. A sensor is a device that reacts to a physical stimulus and measures a property based on this signal [6]. Numerous types of sensors (e.g. cameras, lasers, ultrasonic devices, thermal devices, load cells) may be used to measure the desired physical property (e.g. acceleration, velocity, distance, heat, light, humidity, pressure) [18]. An accelerometer can for example measure a voltage which is proportional to a force (and thus acceleration) working on the sensor [2]. By calibrating the accelerometer, the measured voltage can be converted into acceleration. The quality of a sensor is defined by several characteristics, such as accuracy (precision and trueness), detection range, sensitivity and for digital sensors, sampling frequency [8]. Figure 2.8 illustrates the meaning of the accuracy properties.

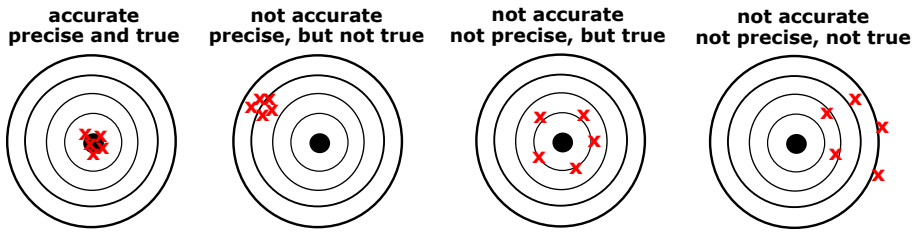

Figure 2.8: Illustration of sensor accuracy.

A good sensor is sensitive to the measured property and insensitive to any other property and does not influence the measured value when being used [8]. It will however sometimes be necessary to post-process the measured signal before passing it into the control. This may be due to unwanted errors, noise or the fact that the measured property needs to be post-processed to obtain data which is more expedient to further process (for example integrating an acceleration signal to a velocity signal). This introduces the theory of digital signal processing and filtering. A digital filter will in some manner perform mathematical operations on a signal to reduce or enhance properties of the signal [22], such as system frequencies. The errors of noise and drift may be addressed by low-pass filters (passes through low frequencies) and high-pass filters (passes through high frequencies), respectively. Both filters are of interest since digital signals may be obtained using both accelerometers and position measuring lasers. Drifting is a common problem when integrating digital signals, as illustrated in Figure 2.9. This is due to accumulation of errors in the integrating process.

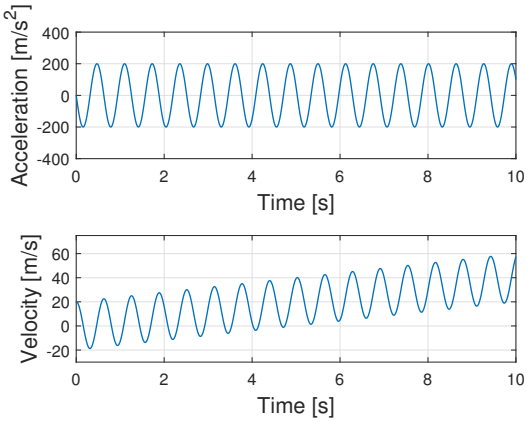

Figure 2.9: Example of drift phenomenon in signal integration from acceleration to velocity.

The derivative of a digital signal does not suffer from drifting since a constant error in the original signal will not affect the resulting signal after derivation. However, the derivation of a digital signal tends to enhance the effect of noise. Therefore, a low-pass filter is often necessary when the signal from a position sensor is used to obtain velocity and acceleration through derivation. *Single pole filters* are good overall recursive filters and may be used to address several digital signal processing issues [22]. A recursive filter is a filter that uses its own previously filtered values in the algorithm, and for single pole filters, one uses the last point only. That makes them computational efficient and simple to implement in programs. Since the output will have a smooth rise/fall towards the level of steady state, they are well suited to cope with drifting [22].

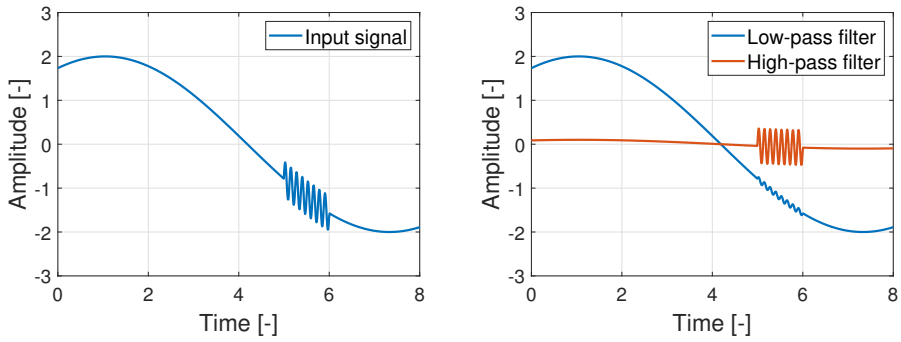

(a) Input signal.

(b) Output signal after filtering.

Figure 2.10: Example of how low-pass and high-pass filters (b) react to a digital input signal consisting of high frequent noise and a low frequent wave.

Figure 2.10 shows how low-pass and high-pass single pole recursive filters react to a signal exposed to high frequent noise and a low frequent wave. The high pass recursion filter

which is used to filter the digital signals from accelerometers is given as [22]

$$y[n] = a_0[n] + a_1x[n-1] + a_2x[n-2] + ... + b_1y[n-1] + b_2y[n-2] + ..., \quad (2.30)$$

where x is the input signal and y is the filtered signal. For a single pole high-pass filter, the constants are given as

$$\begin{aligned} a_0 &= (1+r)/2 \\ a_1 &= -(1+r)/2 \\ b_1 &= r, \end{aligned} \quad (2.31)$$

whereas for a low-pass filter:

$$\begin{aligned} a_0 &= 1-r \\ b_1 &= r, \end{aligned} \quad (2.32)$$

where r is the filter coefficient given as

$$r = e^{-2\pi f_c/f_s}, \quad (2.33)$$

with f_c and f_s as cutoff frequency and sampling frequency, respectively [22]. The cutoff frequency determines what threshold to set on the frequency content to pass through the filter.

2.6 Evaluating Energy in Vibrating Systems

Loss of energy per time is a natural approach when evaluating the effect of dampers. The energy of a vibrating system consists of potential energy, U, and kinetic energy, T. At any given time, the energy in the system is given by

$$E = U + T = \frac{1}{2}ku(t)^2 + \frac{1}{2}m\left(\frac{du}{dt}\right)^2. \quad (2.34)$$

The energy of the oscillating system may be estimated using the envelope function describing the general decrease of amplitude as a function of time. This is due to the fact that the energy of the system at any point where the displacement is at a peak - meaning the velocity is zero - the total energy of the system is only dependent on the potential energy and hence the amplitude and stiffness of the system. Any time the system is between two consecutive peaks, it is known that the energy of the system is smaller than that of the first peak and larger than that of the second peak by the law of conservation of energy. This means that the energy in the system can be approximated as

$$E \approx \frac{1}{2}kA^2. \quad (2.35)$$

$A = A(t)$ describes the envelope function passing through the peaks of $u = u(t)$.

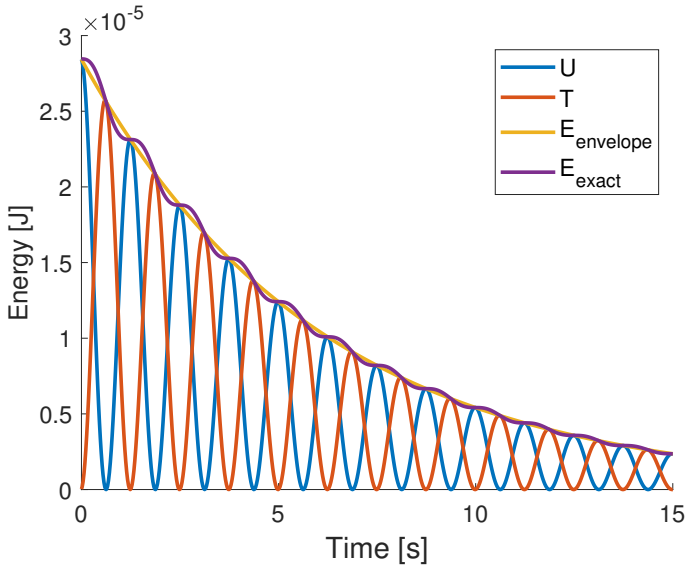

Figure 2.11: Example of energy in a vibrating SDOF system.

The motivation for this simplification is that it makes it easier to compare the results for different dampers. Furthermore, calculating the energy using Equation 2.34 requires high accuracy when monitoring the vibrating system, since the method is sensitive to time delay, especially for high frequencies. Figure 2.11 shows how the energy in an oscillating SDOF system decreases over time due to damping in the system. It is clear from the figure that the energy obtained using the envelope function as in Equation 2.35 gives a good approximation of the total energy.

Chapter 3

Methods

The approach for the project was as follows:

- Study general structural dynamics and active damping theory.
- Set up a physical test rig in the lab, for testing different types of active damping applications. This included a cantilever beam as well as a beam fixed with respect to translations and rotations in both ends.
- Develop a program in MATLAB, simulating the vibrating beams of the test rig, simplified as SDOF systems. This could be used to predict the efficiency of different actuators and control algorithms.
- Perform experiments on the test rig with sensors, actuators and control algorithms to optimize the application.

3.1 MATLAB Simulation

In order to test numerous damping applications in a time efficient way, a simulation code was written in MATLAB. The simulation made it possible to gain knowledge of which parameters that affect the ability to damp out vibrations most efficiently. The code was simplified as a SDOF system to simulate both the cantilever beam and fixed-ends beam of the test rig described in Section 3.2.

3.1.1 Code Structure

The cantilever beam and fixed-ends beam were discretized with one node at each end, and with one node at each end and a center node, respectively. The modal mass of the system was calculated using mass lumping which yields half the mass of the beam in both cases. Furthermore, the code was written with the ability to change the structural properties such

as the fundamental frequency and the damping ratio. The stiffness and damping coefficient were calculated through the relations

$$k = m_{modal}(2\pi f_{target})^2, \tag{3.1}$$

$$c = 2\xi\sqrt{km}, \tag{3.2}$$

where f_{target} and ξ are the fundamental frequency and the damping ratio, respectively. The modal mass depends on the length of the beam which again depends on the defined natural frequency through Equation 3.9. To maintain a tidy structure of the simulation, the code was developed with a main script (*systSim.m*) using functions with specific tasks. The main script and its functions can be found in the Appendix. When using the simulation, one may assign how the vibrations should be induced. This can be done by either specifying an initial displacement, velocity or acceleration, or by assigning external loads throughout the simulation. These external loads are assigned as a function of time and can be either a sine-wave, a random signal or a combination of these. One can also decide what actuator to test, which specifications are returned from the function *getActuator* or *getSolenoid* depending on the choice of actuator. The specifications include mass, stroke length and maximum acceleration, velocity and force. The system variables and the sample frequency may be specified along with the constants of the feedback algorithm, described in Section 2.5.1. The simulation is carried out by the Newmark-beta method where the time increment, Δt, is set sufficiently low to ensure convergence. The force from the actuator is included as the external load F in the SDOF equation of motion solved by the Newmark-beta method specified in the following equations:

$$\ddot{u}_{n+1} = \frac{1}{m}(-c\dot{u}_n - ku_n + F), \tag{3.3}$$

$$\dot{u}_{n+1} = \dot{u}_n + (1-\gamma_{nb})\Delta t\ddot{u}_n + \gamma_{nb}\Delta t\ddot{u}_{n+1}, \tag{3.4}$$

$$u_{n+1} = u_n + \Delta t\dot{u}_n + \frac{1}{2}\Delta t^2((1-2\beta_{nb})\ddot{u}_n + 2\beta_{nb}\ddot{u}_{n+1}), \tag{3.5}$$

where $\gamma_{nb} = 0.5$ and $\beta_{nb} = 0.25$. The following list sums up the purposes and tasks of the different scripts and functions of the simulation.

- *systSim.m* - The main script of the simulation. One can here specify loads and initial conditions of the system. The result for the system and actuator movements are plotted in the end.
- *getSolenoid.m* - The solenoid database. One may here add different solenoid models with its specifications. This includes stroke range, mass of moving piston, total mass and the force the solenoids may provide as a function of stroke.
- *getActuator.m* - The database for all actuators that are not solenoids. One may here add different actuator models with its specifications. This includes stroke range, mass of moving piston, total mass and maximum velocity, acceleration and force.

- *beamData.m* - Calculates the beam properties with respect to desired fundamental frequency and beam configuration (cantilever or fixed-ends).

- *regulator.m* - Calculates the recommended acceleration, later multiplied by the piston mass to obtain the force in accordance with Equation 2.24.

- *actuator.m* - This function implements the actuator restrictions in the simulation.

- *newmark_getResponse.m* - This function includes the Newmark numerical method described above and solves the system with respect to the dynamic parameters and the input force of the actuator. The displacement, velocity and acceleration of the system are calculated, thus this function also works as the sensor.

3.1.2 Experiments for Obtaining Solenoid Specifications

One particular solenoid was used for the experiments throughout this project. It was necessary to investigate the amount of force this solenoid could provide to the structure when turned on and off. By knowing the force curve one could predict the effect of solenoids as AMD (active mass damper) in the MATLAB simulations for comparison with the physical testing. Like described in Chapter 2, the solenoid will provide a varying force, depending on duty cycle and stroke, that means the ratio of on-time, and where in the coil the piston is placed. The stroke equals zero when the solenoid is in on-state, that means fully compressed in the coil. This means that the piston will move from right to left in the graph of Figure 3.1 when turned on and travels from off-state to on-state. With the data available, the following method was used to predict the force curve when the solenoid contracted from off-state to on-state:

- The maximum force value at 50% duty cycle and zero stroke was registered from the solenoid datasheet [1].

- The force at the end of the stroke (towards the right side of the force-stroke plot) was assumed to be 10% of the force at zero stroke, based on the solenoid datasheet [1].

- This gave two points in the force-stroke plot, [$stroke = 0$,$Force = F_{max}$] and [$stroke = stroke_{max}$,$Force = 0.1F_{max}$].

- The curve fit function of MATLAB was used to predict the graph on an exponential form, $Force = \alpha \cdot e^{\eta \cdot Stroke}$. The constants α and η were registered.

The estimated solenoid force as a function of stroke when traveling from off-state to on-state are shown i Figure 3.1.

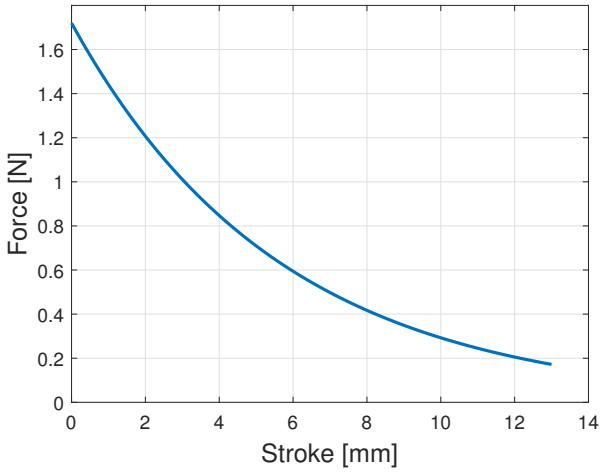

Figure 3.1: Estimated solenoid force as a function of stroke when the piston travels from off-state to on-state, not including gravitational force of the piston and spring force.

However, other forces come into play when calculating the total force induced on the structure. When the solenoid is placed vertically, like in Figure 3.13a, the gravitational force needs to be added, and the spring force needs to be subtracted. The latter demands that the spring stiffness, k, is known, assuming a constant spring stiffness. This value was also necessary in order to study the amount of force the solenoids provided to the structure when going from on-state to off-state, with the aid of Hooke's law,

$$F_{spring} = ku, \tag{3.6}$$

where u is the spring displacement. When calculating the force created when going from on-state to off-state, the gravitational force needs to be subtracted, since the piston now is moving vertically upwards. The stiffness of the solenoid spring was found through testing. Three different mass loads were put on the spring and the displacements were recorded. The linear curve fit function of MATLAB was used to obtain k_{spring}. Mathematically, the forces induced on the structure when the solenoid travels from off-state to on-state, and from on-state to off-state is described by:

$$\begin{aligned} F_{ON} &= F_{solenoid}(stroke) + F_{gravitation} - F_{spring} \\ F_{ON} &= F_{solenoid}(stroke) + m_{piston}g - k_{spring}u \end{aligned} \tag{3.7}$$

$$\begin{aligned} F_{OFF} &= F_{spring} - F_{gravitation} \\ F_{OFF} &= k_{spring}u - m_{piston}g \end{aligned} \tag{3.8}$$

k_{spring} can not be calculated as $stroke_{max} - stroke$, since the spring is compressed in the off-position at $stroke_{max}$. Figure 3.2 and 3.3 are the graphical solutions of Equations 3.7 and 3.8 and show the force from the solenoid on the structure, when the piston went

from off-state to on-state, and from on-state to off-state, respectively. For this particular solenoid, the maximum stroke was $stroke_{max} = 13mm$. Note that the two forces F_{ON} and F_{OFF} in reality will act in opposite directions, thus implying that the forces presented numerically and graphically here represent the absolute values.

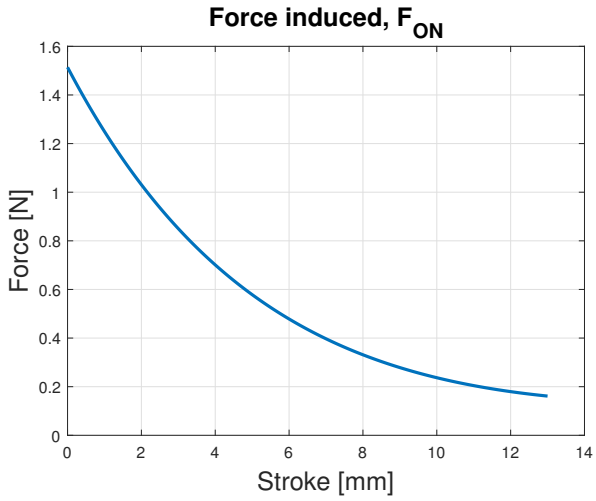

Figure 3.2: Force induced as a function of stroke when solenoid is turned on.

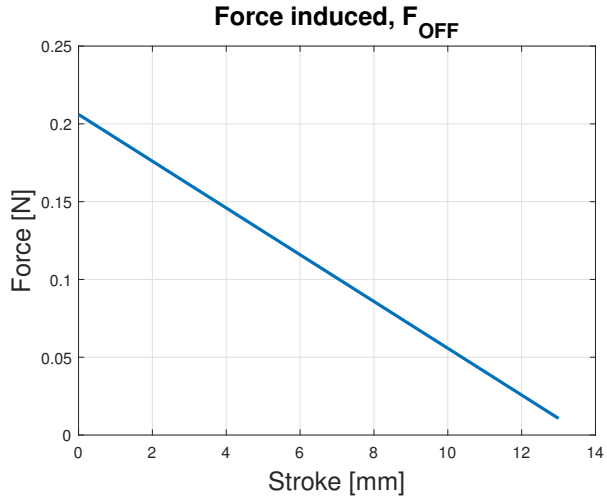

Figure 3.3: Force induced as a function of stroke when solenoid is turned off.

By studying Figure 3.2 and 3.3, it is evident that the solenoid is significantly more powerful when going from off to on-state than the opposite way around. Considering this, it would be more expedient to place the solenoids upside down so the gravitational force would

be added to the on-off stroke and subtracted from the off-on stroke to even out the force curves. However, due to the solenoids lack of power in the off-position at $stroke_{max}$, it was necessary to orient the solenoids like seen in Figure 3.13, to start the motion. Table 3.1 sums up the specifications obtained for the solenoid through testing and curve fitting.

-	**Solenoid**
Spring Stiffness, k $[N/mm]$	0.0150
α	1.72
η	-0.1771

Table 3.1: Experimental force parameters for solenoid.

The solenoid force data obtained by the methods described in this section was used in the MALTAB code to accurately predict the forces from a solenoid in the simulations.

3.1.3 Verification

The main goal of the simulation code was to be able to test various actuators and their ability to damp out vibrations in structures with different dynamical properties, such as natural frequency and damping ratio. To ensure that the results from the simulation were accurate and represented a dynamical SDOF system correctly, the simulation was run with different values for both the natural frequency and the damping ratio. All of the verification tests were run with the SDOF system vibrating freely without interaction from an actuator. One test of importance is where $\xi = 0$. This test ensures that the time increment chosen for the simulation is sufficiently small to prevent divergence throughout the simulation. A time increment of $\Delta t = 10^{-6}s$ was found sufficiently small to ensure convergence. To further verify the ability to simulate damping in a satisfactory manner, the results from a simulation compared to a sine-wave as in Equation 2.6, is presented in Figure 3.4. The parameters of the sine-wave are $A = 0.01$ m, $\omega = 2\pi \cdot 20$ rad/s, $\xi = 0.01$ and $\phi = \pi/2$. The simulation was run with the same values and the results are close to identical, indicating that the simulation is well suited to describe a naturally damped oscillating system. It is also desirable that the simulation reproduces the defined natural frequency. In Figure 3.5, the simulation result using $f_{target} = 20Hz$ and $\xi = 0.02$ is shown along with its spectral density, calculated using the FFT (Fast Fourier Transform) function in MATLAB. It can be seen that the simulation code generates good results regarding the system's natural frequency, which is important to ensure that the simulations run are accurate and reliable.

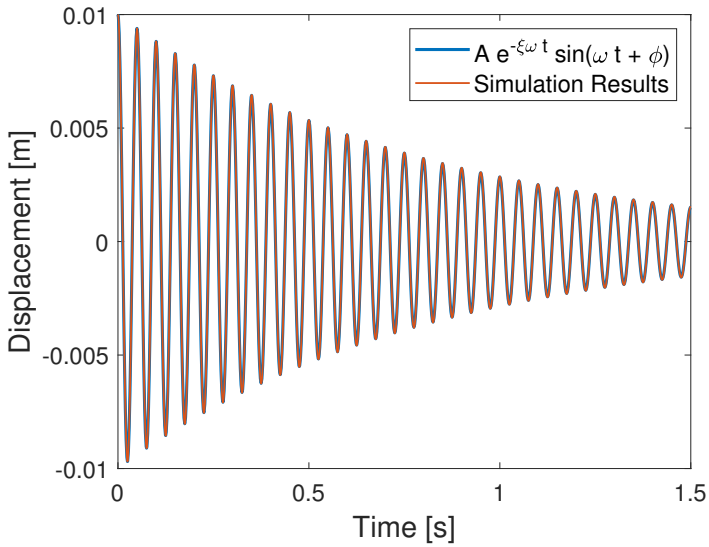

Figure 3.4: Simulation compared to a damped sine-wave.

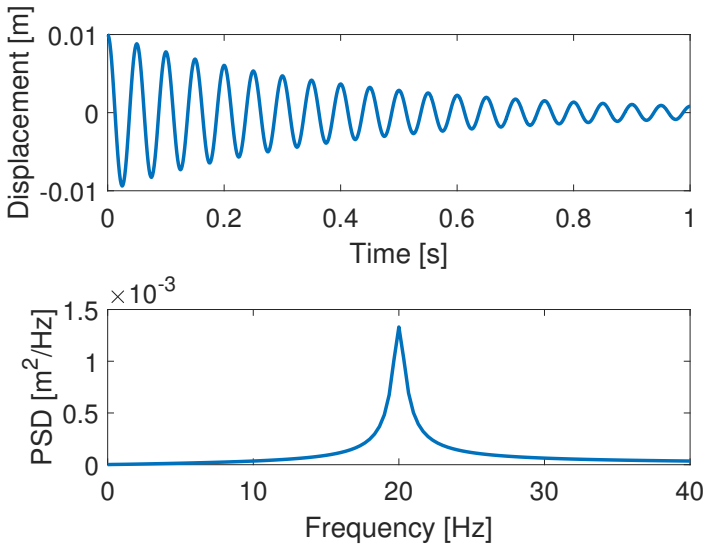

Figure 3.5: Verification of natural frequency of system in simulation.

3.2 Test Rig

In order to test the active damping prototype and the different control algorithms, a test rig was developed in the laboratory of the Department of Structural Engineering. The purpose of this was to simulate the frequencies of vibration one typically observe when testing the bridge models in the wind tunnel. The rig is depicted in Figure 3.6, and its properties can be found in Table 3.2. The dimensions were chosen to be able to simulate frequencies from 10 to $30Hz$. As seen in Figure 3.6, the test rig consists of two beam configurations, a cantilever beam and a beam fixed with respect to translations and rotations in both ends (from now called a *fixed-ends* beam).

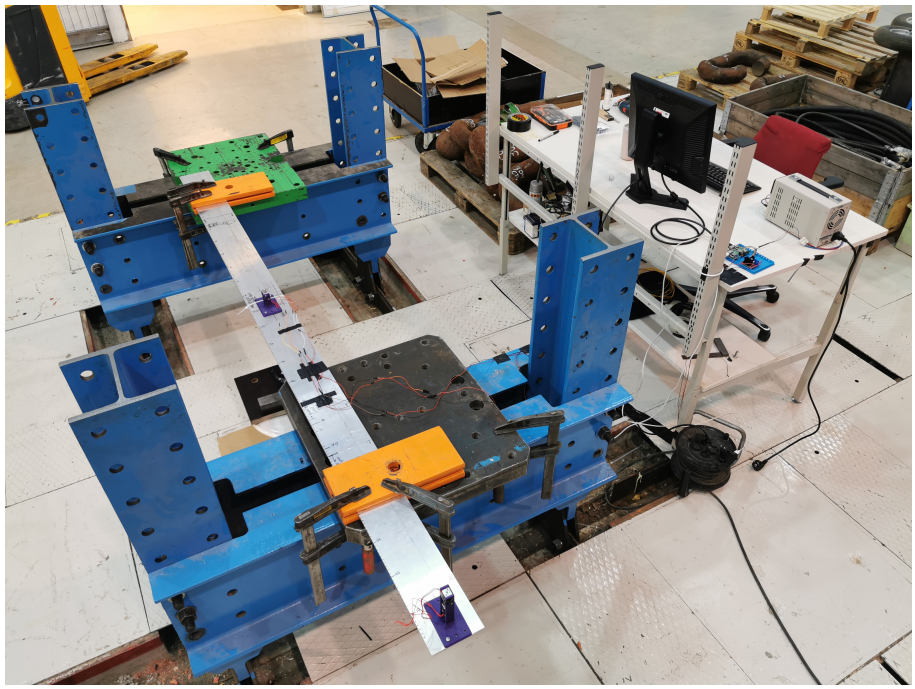

Figure 3.6: Test rig in the laboratory. The two dampers in purple casing show where the dampers were placed when tested on fixed-ends and cantilever beam.

Property	**Value**
Width	$125mm$
Height	$8mm$
Density	$2700kg/m^3$
Young's Modulus	$69000MPa$

Table 3.2: Properties of aluminum test beam.

Aluminum was chosen in order to obtain a total mass of approximately $5kg$ for a beam length with an analytical natural frequency of $20Hz$. This weight was chosen in accordance with a typical mass of a bridge section model [20]. In addition, aluminum is both affordable, available and easy to machine to desired dimensions. By moving the orange steel plates, it was possible to vary the length of both the fixed-ends and cantilever beam. By varying the length of the beam, one can control the fundamental frequency of the beam to correspond to the frequencies one obtain in the wind tunnel. The analytical formula for the natural frequencies of a fixed-ends beam as well as a cantilever beam is given as [23]

$$f_n = \frac{K_n}{2\pi}\sqrt{\frac{EI_y}{bh\rho L^4}}, \tag{3.9}$$

where E is Young's modulus, I_y is the moment of inertia, b and h are the width and height of the cross section, ρ is the mass density, L is the length of the beam and K_n is a constant depending on boundary conditions. K_n is given in Table 3.3 for the first 5 natural frequencies of the two beam set ups.

	$\mathbf{K_{n,fixed-ends}}$	$\mathbf{K_{n,cantilever}}$
Mode 1	22.4	3.52
Mode 2	61.7	22.0
Mode 3	121	61.7
Mode 4	200	121
Mode 5	299	200

Table 3.3: Constants in Equation 3.9 for natural frequencies of fixed-ends and cantilever beam [23].

To test if the calculated natural frequencies corresponded to the measured frequencies of the aluminum beam, an experiment was carried out on the fixed-ends beam, with no damper present. A MPU-6050 accelerometer with a sampling frequency of 100 Hz was attached to the midpoint and was used to measure the beam vibration in a time series of one minute. This particular accelerometer was used since this test was carried out at an early stage in the project, when applications for using a more expensive accelerometer with a higher sampling frequency, were yet to be carried out. This accelerometer was however considered to be sufficient to detect the fundamental frequency of the beam, and to determine its damping ratio. A gentle push was applied four times during this minute with a 15 second pause. A FFT function in MATLAB was used on the collected data to identify the measured frequencies. Figure 3.7 shows the test series and the corresponding spectral density of the test with $L = 2.040m$, meant to simulate a fundamental frequency of $10Hz$. One can observe the dominating peak in the specter at approximately 11 Hz, which is the experimental value of the fundamental frequency. The two other peaks represent the second and third natural frequency of the beam with this particular length.

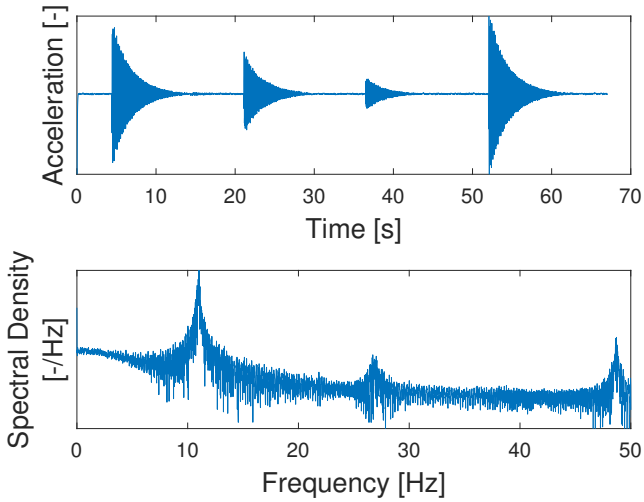

Figure 3.7: Acceleration as a function of time and its Fourier Transform for a fixed-ends beam of length $L = 2.040m$. The response specter is presented logarithmic on the y-axis.

Figure 3.8 illustrates how the analytically calculated natural frequencies of the beam varies with the length of the beam. It is also compared to the experimentally values for the natural frequencies.

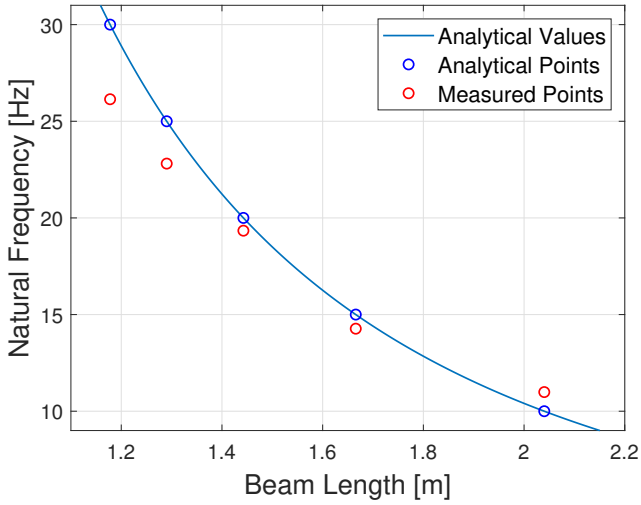

Figure 3.8: Comparison between analytical and measured values of fundamental frequencies of fixed-ends beam in test rig.

It is evident from the figure that the natural frequencies obtained by FFT differs slightly

from the analytically calculated natural frequencies. The figure also shows that the difference tends to increase as the beam length decreases. This can be explained by the fixed ends which in reality not are perfectly fixed, which decreases the stiffness of the system. As the beam lengths decreases, the effect of these non perfect fixed ends becomes more significant to the dynamical properties of the beam. Further, it can be seen in Figure 3.6 that parts of the beam is sticking out as the cantilever beam. A shorter fixed-ends beam means a longer cantilever beam. As the supports at the orange ends are not perfectly fixed, a longer cantilever beam will increase damping of the fixed-ends beam and reduce its stiffness. However, the results show that the beam lengths are sufficient to generate the natural frequencies desired.

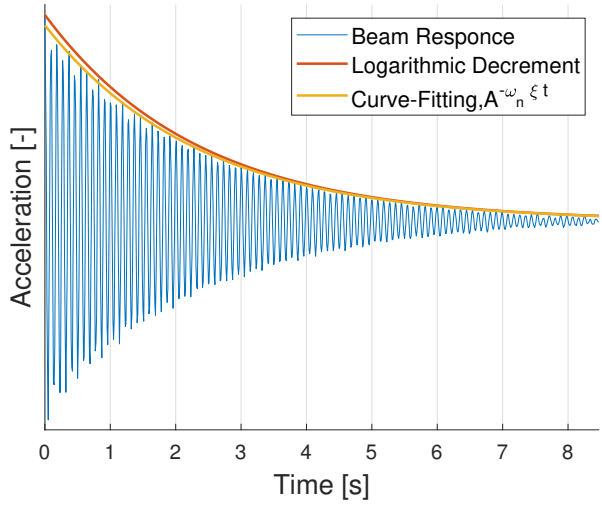

Figure 3.9: Damping ratio calculated with curve fitting and logarithmic decrement.

To evaluate the damping of the fixed-ends beam of the test rig, the damping ratio was calculated by curve fitting and by logarithmic decrement. As shown in Figure 3.9, the amplitude of the oscillations are not strictly decreasing. This may be caused by the sampling frequency being too low or the fact that multiple modes affect the displacement. The logarithmic decrement was calculated for all pairs of successive peaks using Equation 2.7. The average logarithmic decrement was then calculated to obtain a more accurate estimate of ξ_{ld} using Equation 2.8 with $\delta = \delta_{average}$. To calculate the damping ratio obtained by curve fitting, ξ_{fit}, a built in function in MATLAB was used along the peaks of the beam response. The fitted curve was constrained by the exponential contribution of Equation 2.6 to obtain the envelope function $A(t) = A_0 e^{-\gamma t}$. The MATLAB function yields values for A and γ, and the relation $\xi_{fit} = \gamma/\omega_n$ was used to obtain the damping ratio. The results of the damping estimation of the fixed-ends beam can be seen in Table 3.4.

$\mathbf{f_{1,a}}$ $[Hz]$	$\mathbf{f_{1,e}}$ $[Hz]$	$\xi_{\mathbf{ld}}$ $[\%]$	$\xi_{\mathbf{fit}}$ $[\%]$	**Length** $[m]$
10	10.99	0.6211	0.6160	2.040
15	14.27	0.5238	0.5825	1.666
20	19.34	0.4005	0.3925	1.443
25	22.81	1.0035	0.9922	1.290
30	26.14	0.4243	0.4347	1.178

Table 3.4: Fixed-ends beam frequencies and damping ratios for various lengths.

This shows that the analytical formula for the natural frequency of the beam is a good prediction of which beam length to choose to predict pre defined natural frequencies. It is reason to believe that this also applies to the cantilever beam design of the test rig. These tests were performed with no damper mounted on the rig. Doing this will add mass to the system and thus lower its fundamental frequency. As the formulas do not perfectly predict the fundamental frequencies - and added mass of the dampers will impact the dynamic properties - it is important to perform pretesting without the active damper acting, but still mounted on the rig, to obtain information about the system of that particular configuration in free vibration for reference to the damped vibration cases.

3.3 Solenoid as Active Damper

In order to gain practical experience of active damping, and test possible actuators for the bridge model application, it was suggested to investigate the use of linear push pull solenoids. Solenoids have several benefits. They are both cheap and easy accessible and can be controlled by a simple control algorithm in the regulator. Figure 3.10 shows a solenoid in off-state and on-state, respectively.

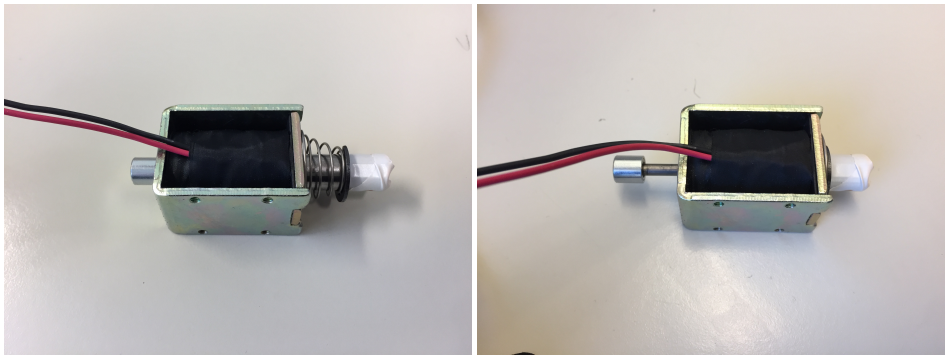

(a) Solenoid in off-state, $stroke = stroke_{max}$. **(b)** Solenoid in on-state, $stroke = 0$.

Figure 3.10: Solenoid in off and on state.

When the coil is subjected to sufficient current, the piston will contract. This process will both load the spring and subject a force on the construction the solenoid is mounted on.

When the current is turned off, the spring will unleash its potential energy and accelerate the piston back to its off-position, thus creating a force on the construction, in the opposite direction of the first process. This is simply based on Newtons third law of equal and opposite counter forces. This means that it will be possible to apply a force in opposite directions to damp out the motion of a vibrating construction. These two forces are however restricted to specific values, depending on the specifications of the solenoid, implying that a feedback algorithm where the force from the actuator is proportional to an obtained signal is impossible. The control algorithm for solenoids is based on threshold values, where the current is turned on or off if a physical instrumented property (e.g. position, velocity and/or acceleration) exceeds a pre-defined value. It was necessary to set up a control system that could both read a sensor signal and provide sufficient current to the solenoid. This system is depicted in Figure 3.11.

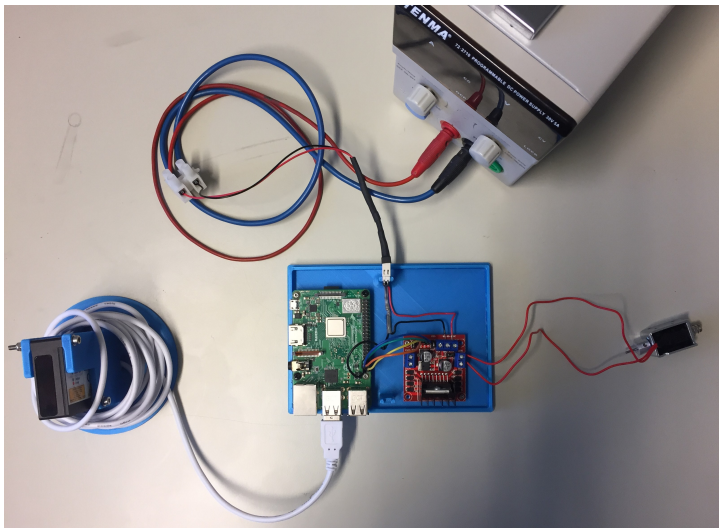

Figure 3.11: Raspberry Pi setup for test of solenoid as AMD.

Raspberry Pi is a series of small computer boards which easily can be programmed to the desired configuration. It is affordable and easy to set up. The model *Raspberry Pi 3 Model B+* was used in this project and contains numerous *general purpose input output* (GPIO) pins to connect the board to other components. The board was connected to a power source, a sensor and a H-bridge. The H-bridge was again connected to one or two solenoids, depending on the tested configuration. The purpose of the H-bridge was to control the current from the power supply and the model called *Dual H-Bridge L298N* was used. The model *ODS USB-150* from DSE was chosen as sensor. This is a distance measuring laser which provides data at a sampling rate of $1kHz$. It provides both ASCII and binary input to the system which easily can be derived to obtain the velocity and acceleration of the structure. Unlike an accelerometer mounted on the structure, a laser placed on solid ground measuring the distance to the structure, will not influence the total mass of the structure, and thus its dynamic properties. The setup with Raspberry Pi, H-

bridge and laser was chosen for the testing of solenoids since it was an efficient way to familiarize with the concept of active damping and decide if more advanced equipment was necessary for further testing. The distance measuring laser was chosen to exclude drifting and potential measuring errors that may occur if an accelerometer is rotated out of the orientation it was calibrated to operate in. The schematic setup is depicted in Figure 3.12. Note that the schematic illustration in Figure 3.12 contains two solenoids, unlike Figure 3.11 with one solenoid only.

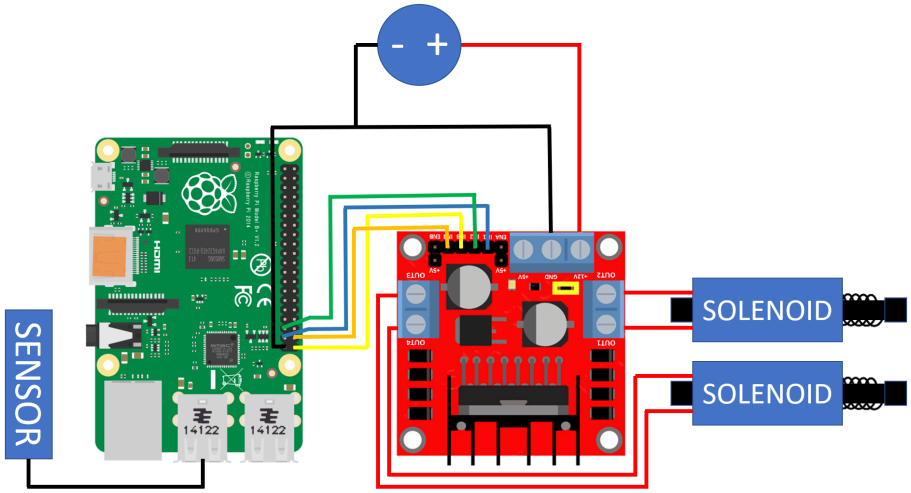

Figure 3.12: Schematic illustration of Raspberry Pi setup for test of solenoid as AMD.

It was decided to test two different solenoid configurations on the test rig. These were use of one single solenoid and two solenoids in serial of the same type, namely the model SD0630 from *RS Components*. The reason for testing two solenoids in serial is that the force in each direction will be approximately the same, whereas with a single solenoid the force by the electromagnet is much larger than the force created by the spring as was discussed in Section 3.1.2. This solenoid has a maximum stroke of $13mm$. The most important specifications may be found in Table 3.5. The two configurations tested are depicted in Figure 3.13.

-	**Solenoid Specs**
Model Name	SD0630
Total Mass	$41.0g$
Moving Mass	$5.5g$
Voltage	$12V$
Maximum Stroke ($stroke_{max}$)	$13mm$
Max Force at 50% duty cycle	$1.7N$

Table 3.5: Specifications of the SD0630 solenoid [1].

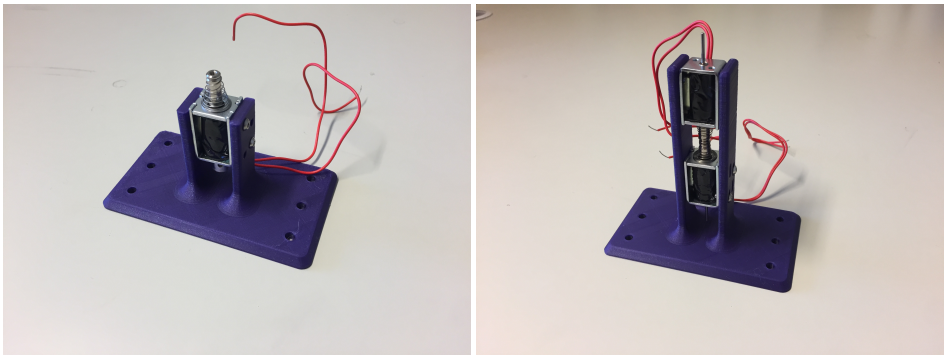

(a) Single solenoid. **(b)** Double solenoid in serial.

Figure 3.13: The two different solenoid configurations tested in their 3D-printed holders.

Holders for the different configurations were manufactured by 3D prints in order to mount the solenoids on the test rig. Figure 3.14 shows an overview of the solenoid experiments.

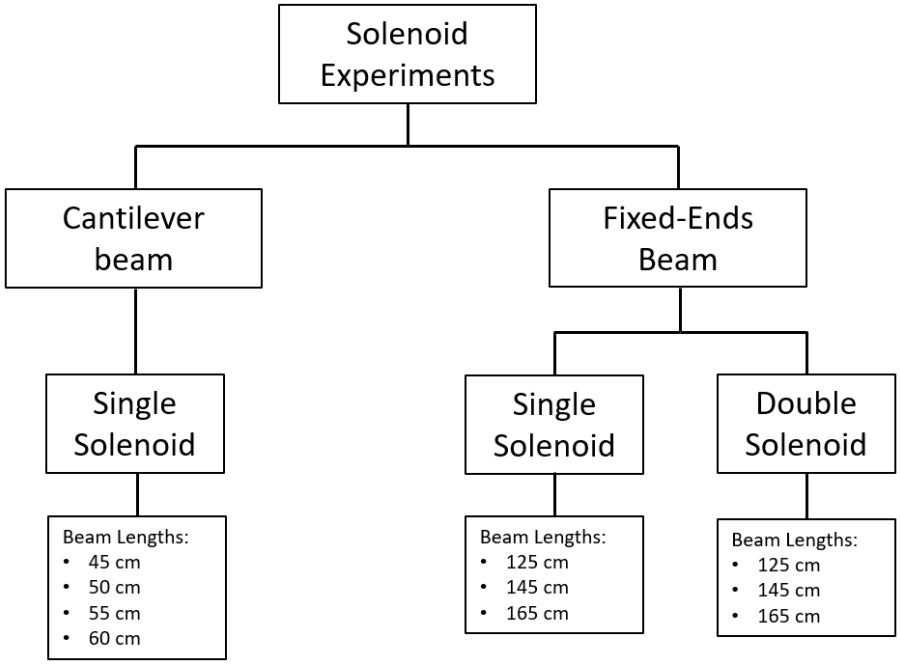

Figure 3.14: Solenoid test plan.

Different control algorithms and threshold values were tested within these configurations as well. As explained in Chapter 2, the direct velocity feedback seems to be the most simple and effective algorithm for active damping configurations. Therefore, the action of the solenoids were based on velocity threshold values. This means that the solenoid

is turned on and contracts when the instrumented velocity reaches a defined value, and is kept turned on until the velocity of the system reaches the same threshold value, but with opposite sign. That gives a velocity threshold (VT) algorithm,

$$Solenoid_{STATE} = \begin{cases} ON, & \text{if } v < -v_{thr} \\ OFF, & \text{if } v > v_{thr} \\ UNCHANGED, & \text{Otherwise} \end{cases} \tag{3.10}$$

where v_{thr} is the defined velocity threshold in the algorithm, and v is the detected velocity of the structure. The greater-than and less-than signs are set in accordance with a positive direction upwards. When the structure moves vertically in positive direction, the solenoid is turned off and the spring will accelerate the piston upwards in the same direction as the structure. This will produce a counter-force from the piston to the solenoid and the structure the solenoid is mounted on, thus creating a downward force opposite to the direction of movement. The exact same procedure happens as the structure is moving downwards, except this time the solenoid will be turned on. The principle for the double solenoid in serial is the same, but the upper solenoid is now placed upside down, meaning that one solenoid will be turned on, while the other will be turned off when the velocity threshold value is exceeded in either positive or negative direction.

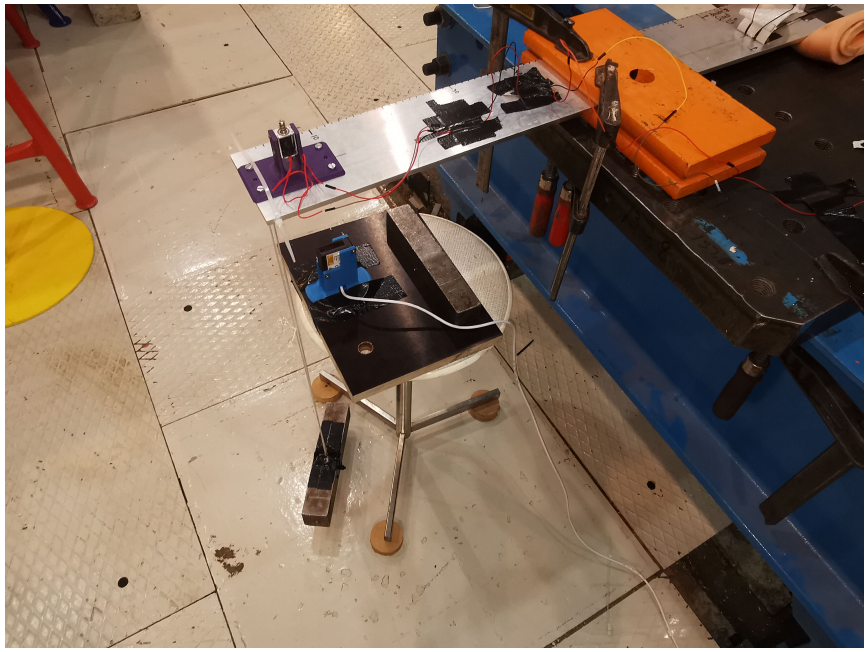

Figure 3.15: Cantilever beam.

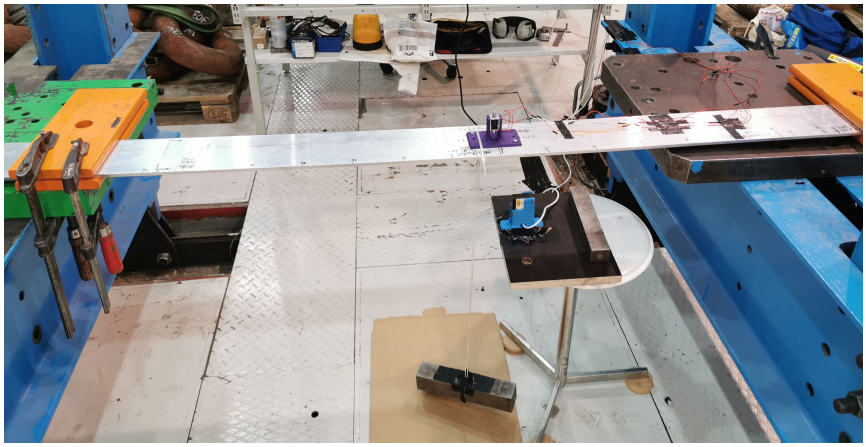

Figure 3.16: Fixed-ends beam.

Figure 3.15 and 3.16 show the general setup for the two beam configurations. A $5kg$ weight was used to set the beams into motion. This was done by attaching the weight to the beam with cable ties and then cut the tie with a pliers at the beginning of each test. This ensured a constant initial displacement for each beam configuration. The laser sensor used for instrumentation can be seen in the blue 3D-printed casing underneath the beam, measuring the distance from solid ground to the moving beam. Ideally, this should be placed right under the point of the active damper, but this turned out to be difficult as space was needed for the weight used for initial displacement. The point of instrumentation was instead placed $5cm$ from the point underneath the damper - for all experiments performed. Since the velocity threshold algorithm uses the derivative of measured displacement to decide on action commands to the damper, filtering was necessary to obtain the desired physical property. The signal from the position sensor was first filtered using the low-pass filter as described in Section 2.5.3, before the velocity was calculated using the values from the filtered position. At last, the acceleration was obtained using the same procedure as used for the velocity. The derivatives are calculated from:

$$v_i = v^*_{i-1} + \frac{u^*_i - u^*_{i-1}}{\Delta t} \tag{3.11}$$

$$a_i = a^*_{i-1} + \frac{v^*_i - v^*_{i-1}}{\Delta t} \tag{3.12}$$

which assumes a constant acceleration from point i to $i+1$. This was considered to be a good approximation with a sampling frequency of $1kHz$. u^*_i, v^*_i and a^*_i denotes the filtered values for the position, velocity and acceleration, respectively.

3.3.1 Cantilever Beam

The first experiments were carried out on a cantilever beam of four different lengths, $45cm$, $50cm$, $55cm$ and $60cm$. Figure 3.17 shows the general setup.

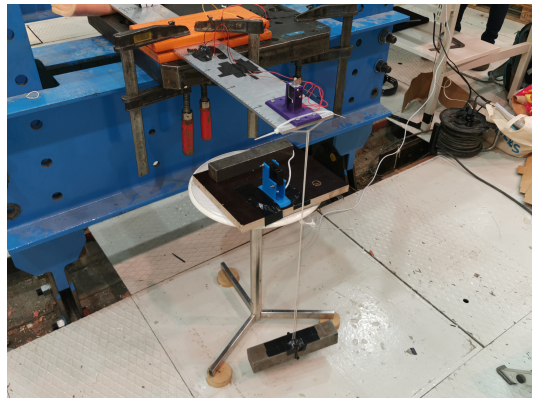

Figure 3.17: Cantilever beam from experiments.

One of the advantages of experiments on a cantilever beam compared to a beam fixed in both ends, is that the cantilever beam will have larger vibration amplitudes than a fixed-ends beam with the same fundamental frequency. This gives a better opportunity to visually observe how effective the damper and its control algorithm really is. The orange plates were attached to the beam with the aid of two clamps to make the fixed point as tight and strong as possible. The leads of the solenoids were taped to the beam, rather than attached straight to the Raspberry Pi, to not impact the system stiffness. The single solenoid configuration was tested on all four lengths.

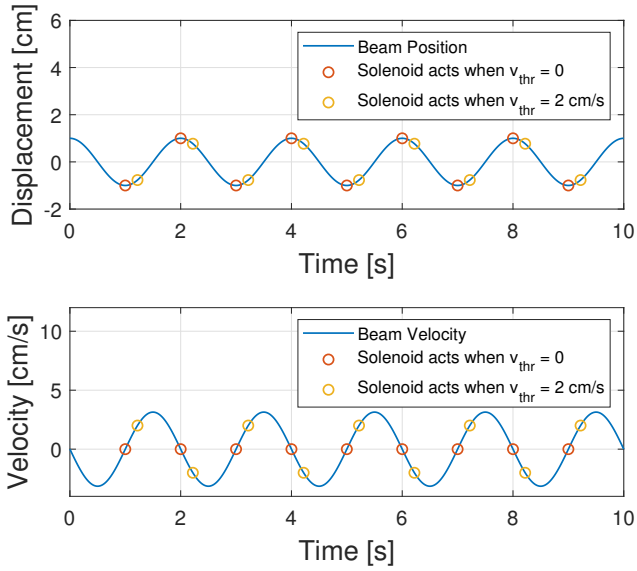

Figure 3.18: Illustrative example of how the velocity threshold algorithm works on an undamped system with an initial displacement of $1cm$.

The velocity threshold (VT) algorithm were used in all experiments, with a threshold value, v_{thr}, varying from 0 to $100mm/s$. Figure 3.18 is presented as an example to show how the VT algorithm works with an initial system displacement of $1cm$. The yellow circles indicates where the solenoid will start acting when the velocity threshold is set to $2cm/s$. Note that the system presented is undamped and that the solenoid acting does not contribute to damping. The plots presented are rather included to illustrate the concept of the algorithm. The cantilever beam experiments were used for optimizing the control algorithm before the tests on the fixed-ends beam, which was regarded as a more realistic test rig setup with respect to the bridge section models.

3.3.2 Fixed-Ends Beam

The next experiments were carried out on a beam fixed in both ends with three different lengths, $125cm$, $145cm$ and $165cm$. Figure 3.19 shows a closeup of the mounted solenoid, the sensor and the 5kg weight connected to the beam with cable tie.

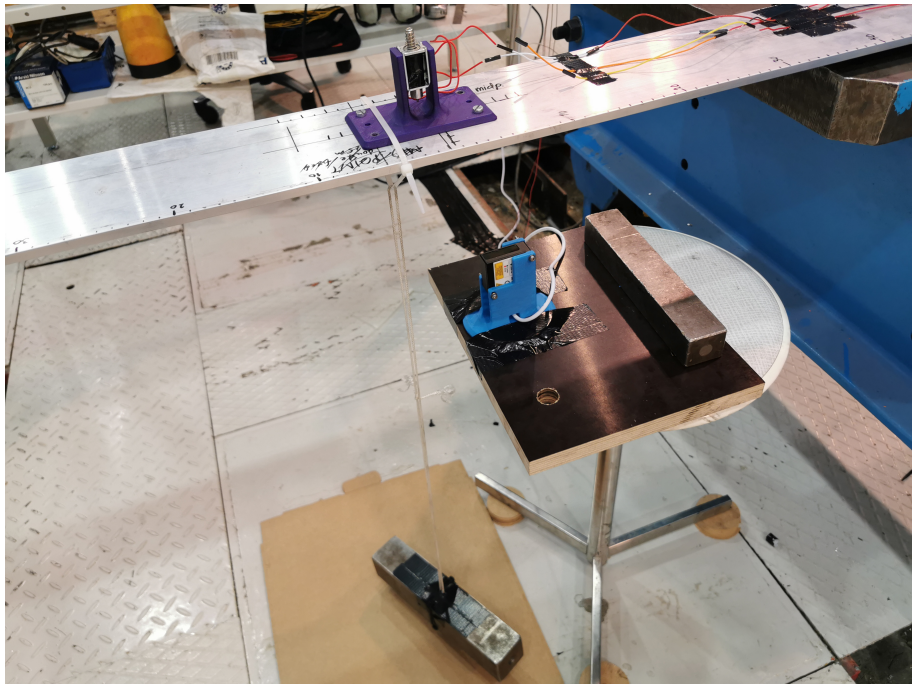

Figure 3.19: Fixed-ends beam from experiments.

This was regarded as a more relevant test compared to the bridge section models, due to weight and boundary conditions. Based on the results of the cantilever beam experiments, a constant velocity threshold of $v_{thr} = 0$ was used throughout the fixed-ends experiments, and the VT algorithm was tested on this configuration too. For the fixed-ends beam experiments, the double solenoid configuration was introduced as well, to test if this was a more efficient damping application. When using a velocity threshold of zero or close to zero, the

solenoid may continue its operation after the vibrations are damped out, since the threshold value is easily reached. This will again set the system in new unwanted vibrations. In order to cut off the solenoid operation before its movements started to excite the bridge more than damp out its vibrations, a velocity-displacement threshold (VDT) algorithm was suggested. This works in the same way as the regular velocity threshold algorithm, except for the introduction of a position threshold, d_{thr}, which indicates a range of displacement values around zero where the solenoid does not act. If the displacement signal registered is within the range $[-d_{thr}, d_{thr}]$ for the last 200 sample points, the solenoid stops acting in accordance with the velocity threshold. 200 sample points are sufficient to detect at least one period for the lowest beam frequencies tested, meaning that the displacement values of the last period of oscillation, needs to be inside the displacement threshold range $[-d_{thr}, d_{thr}]$ before the solenoid stops acting.

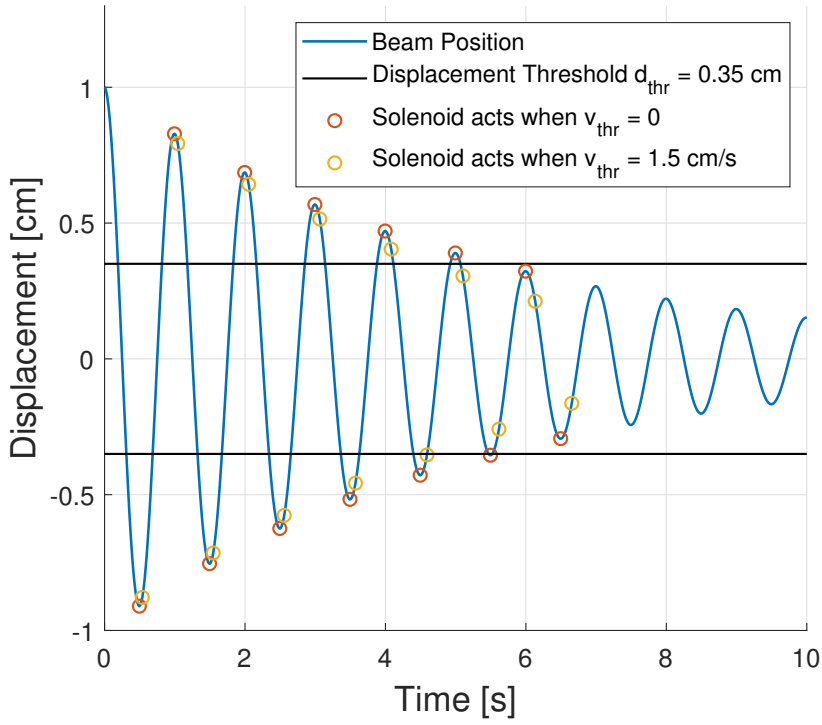

Figure 3.20: Illustration of how the velocity-displacement threshold algorithm stops the solenoid from acting once a whole period of oscillation is within the range $[-d_{thr}, d_{thr}]$

Figure 3.20 illustrates how the VDT algorithm prevents the solenoid from acting and hence from exiting the bridge when at least one whole period of oscillation is within the boundaries of the displacement threshold. The figure also shows how the behaviour of the solenoid changes when the VDT is used in combination with $v_{thr} = 0$ and $v_{thr} > 0$. The particular values for d_{thr} and v_{thr} was chosen for illustrative purposes.

The experiments on the fixed-ends beam were carried out in the following way.

- Three beam lengths were used - $125cm$, $145cm$ and $165cm$. All experiments were carried out for both the single and double solenoid configuration at each length before changing the beam length.
- The VT algorithm with $v_{thr} = 0$ was tested for all beam lengths with both the initial displacement of the 5kg weight and with a random load. The random load was induced by human force, by randomly tapping and shaking the beam for 8 seconds.
- The VDT algorithm was tested on all beam lengths, with both the initial displacement of the 5kg weight and with a human induced random force. The value of the displacement threshold, d_{thr}, was varied with each beam length, since the displacement range is smaller for shorter and stiffer beams. The velocity threshold was set to $v_{thr} = 0$ for all experiments on the fixed-ends beam, for both the VT and VDT algorithm.

3.3.3 Evaluating the Damping Performance

Several calculations were carried out in the post-processing of results to quantify the damper performance. The dissipation of energy for an oscillating system per time is not constant. However, it is useful to look at the percentage of dissipated energy per time since it is easy to obtain and provides an intuitive measurement of how good the active damper performs. The following method was used.

- The beam displacement was logged. The value of the first peak was registered as the value A_0, at time $t_0 = 0$.
- The time it took for the envelope function of the system $(A(t))$ to reach an amplitude equal to 10% of A_0 was registered as $t_{10\%}$. The value of this amplitude was denoted $A_{10\%}$.
- The difference in energy in these two points was simply calculated as

$$\Delta E = E_0 - E_{10\%}, \tag{3.13}$$

  where the energy was calculated with Equation 2.35.

- The percentage of energy dissipated per unit time over this period was calculated as

$$\%\Delta E = \frac{100(E_0 - E_{10\%})}{E_0 t_{10\%}}. \tag{3.14}$$

  The quantity $\%\Delta E$ will the have the unit [%/s].

The decision of evaluating the damper at a point of 90% reduction in amplitude was made for two reasons. This amplitude was regarded large enough so the effect of sensor noise could be neglected. Furthermore, a 90% reduction in amplitude means a 99% reduction

in energy, since the energy is proportional to displacement squared, in accordance with Equation 2.35. Commonly, the damping ratio is used to quantify the damping of an oscillating system. The damping ratio may however be hard to determine in a system with forced damped vibration which does not necessarily vibrate with an exponential decay. To be able to compare the damping of the system oscillating freely and the damping when the system was damped by an actuator, an equivalent damping ratio, ξ_{eq}, was calculated based on Equation 2.6. The envelope function of a free vibrating system is given as

$$A(t) = A_0 e^{-\omega_n \xi t}, \tag{3.15}$$

whereas the energy is given as

$$E(t) = \frac{1}{2} k A(t)^2. \tag{3.16}$$

At time $t = t_{10\%}$, the energy is given as

$$E_{10\%} = \frac{1}{2} k A_{10\%}^2. \tag{3.17}$$

Combining Equation 3.15 and 3.17 and solving for ξ gives the equivalent damping ratio as

$$\xi_{eq} = -\frac{ln\left(\frac{2E_{10\%}}{kA_0^2}\right)}{2\omega_n t_{10\%}}. \tag{3.18}$$

This equivalent damping ratio describes what the damping ratio must be for the system to have the same value for $\%\Delta E$ and $A_{10\%}$ at time $t_{10\%}$ if it was to oscillate as a system in free vibration.

Chapter 4

Results

To analyze the solenoid's ability to damp out vibrations, a series of tests were conducted. The beam lengths were chosen to obtain fundamental frequencies around $15 - 25Hz$. Table 4.1 contains data about the structural and dynamical properties for each of the beam configurations. For each beam setup, f_n was obtained using FFT, and ξ through curve fitting as described in Section 2.2. The modal mass, m_m, was calculated using mass lumping which for a cantilever or a fixed-ends beam simplified as a SDOF system, will be half the total beam mass. The damping coefficient, c, was calculated by combining Equation 2.3 and 2.4, and k was calculated by rearranging Equation 2.2 with $\omega_n = 2\pi f_n$. In the results presented in this chapter, u_f and u_a denotes displacement of a beam in free vibration and a beam damped by an AMD, respectively. The same indices applies for the corresponding amplitudes, A_f and A_a.

Beam Type	**Length [m]**	$\boldsymbol{f_n[Hz]}$	$\boldsymbol{\xi}[\%]$	$\boldsymbol{m_m[kg]}$	$\boldsymbol{c[kg/s]}$	$\boldsymbol{k[N/m]}$
Cantilever	0.45	24.408	0.33	0.6075	0.6332	15504
Cantilever	0.50	20.129	0.34	0.6750	0.6215	12301
Cantilever	0.55	16.719	0.32	0.7425	0.4958	7873
Cantilever	0.60	14.870	0.25	0.8100	0.3495	5986
Fixed-Ends	1.25	23.471	0.24	1.6875	1.2353	38239
Fixed-Ends	1.45	18.111	0.28	1.9575	1.2535	25812
Fixed-Ends	1.65	14.800	0.25	2.2275	1.0313	19655

Table 4.1: Properties of the tested beam configurations when allowed to vibrate freely after a stable initial load of 5 kg was removed instantaneously. The single solenoid was mounted on the beams in these experiments, but turned off.

4.1 Cantilever Beam of Length 45 cm

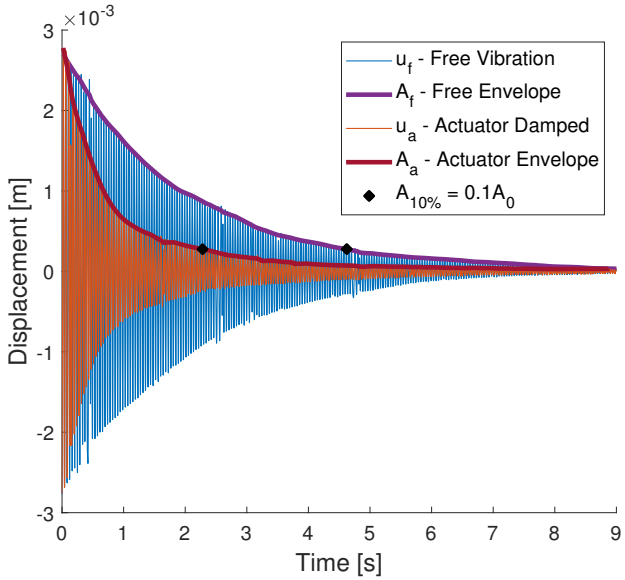

Figure 4.1: Free vibrations and the most effective damping result using the single solenoid configuration with $v_{thr} = 0$ in the VT algorithm on the cantilever beam of $L = 45cm$.

$v_{thr}[mm/s]$	$A_0[mm]$	$t_{10\%}[s]$	$\xi_{eq}[\%]$	$\Delta E/s[mJ/s]$	$\%\Delta E[\%/s]$
Free	2.57	4.419	0.33	11.44	22.40
0	2.76	2.289	0.63	25.70	43.24
2	2.36	2.581	0.55	17.04	38.36
4	2.53	2.481	0.58	20.10	39.91
6	2.52	2.641	0.54	18.99	37.49
8	2.76	3.228	0.44	18.36	30.67
12	2.60	3.726	0.38	14.20	26.57
20	2.58	N/A	N/A	N/A	N/A
30	2.51	N/A	N/A	N/A	N/A
40	2.62	N/A	N/A	N/A	N/A
50	2.82	5.360	0.27	11.47	18.47
60	2.45	4.859	0.30	9.57	20.37
80	2.51	3.389	0.42	14.41	29.21
100	2.77	3.485	0.41	17.04	28.41

Table 4.2: A selection of data obtained on the cantilever beam of $L = 45cm$ using the single solenoid configuration and the VT algorithm.

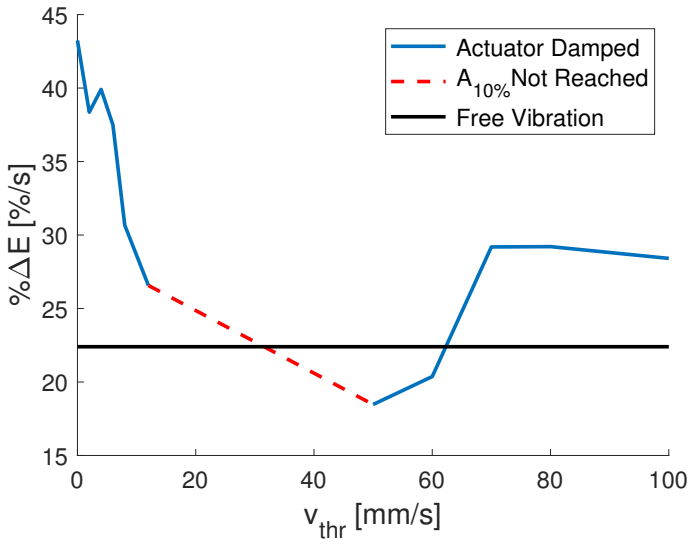

Figure 4.2: Average percentage of energy damped out for a selection of values for v_{thr} in the VT algorithm for the cantilever beam of $L = 45cm$.

Figure 4.1 shows the beam vibrating freely, compared to the best damping result for the VT algorithm which was obtained with a threshold value of $v_{thr} = 0$. 90% reduction in amplitude was obtained in half the time for the most effective algorithm compared to free vibration. Table 4.2 shows the performance of a selection of threshold values in the VT algorithm. For a set of values, the point of 90% reduction in amplitude was not obtained. For certain values, the application even performs worse than the system in free vibration. Figure 4.2 shows the average percentage energy decay per second in the time period between t_0 and $t_{10\%}$. Lower values of v_{thr} seems to be more efficient than higher values of v_{thr}.

4.2 Cantilever Beam of Length 50 cm

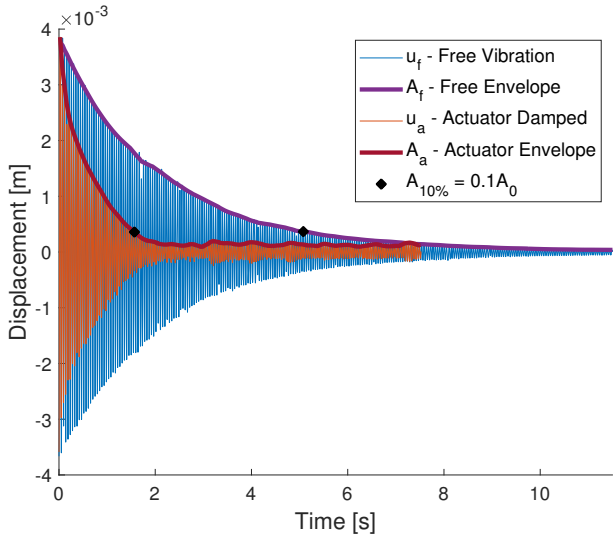

Figure 4.3: Free vibrations and the most effective damping result using the single solenoid configuration with $v_{thr} = 6mm/s$ in the VT algorithm on the cantilever beam of $L = 50cm$.

$v_{thr}[mm/s]$	$A_0[mm]$	$t_{10\%}[s]$	$\xi_{eq}[\%]$	$\Delta E/s[mJ/s]$	$\%\Delta E[\%/s]$
Free	3.66	5.003	0.34	16.35	19.79
0	3.95	1.771	0.96	54.25	55.90
2	3.94	2.028	0.83	47.60	48.82
4	3.58	1.875	0.90	42.70	52.79
6	3.59	1.572	1.07	51.32	62.99
12	3.52	2.183	0.77	35.33	45.35
20	3.50	2.798	0.60	27.58	35.38
30	3.51	N/A	N/A	N/A	N/A
40	3.34	N/A	N/A	N/A	N/A
50	3.44	N/A	N/A	N/A	N/A
60	3.53	N/A	N/A	N/A	N/A
80	3.60	4.862	0.35	16.46	20.36
100	3.66	4.406	0.38	18.89	22.47

Table 4.3: A selection of data obtained on the cantilever beam of $L = 50cm$ using the single solenoid configuration and the VT algorithm.

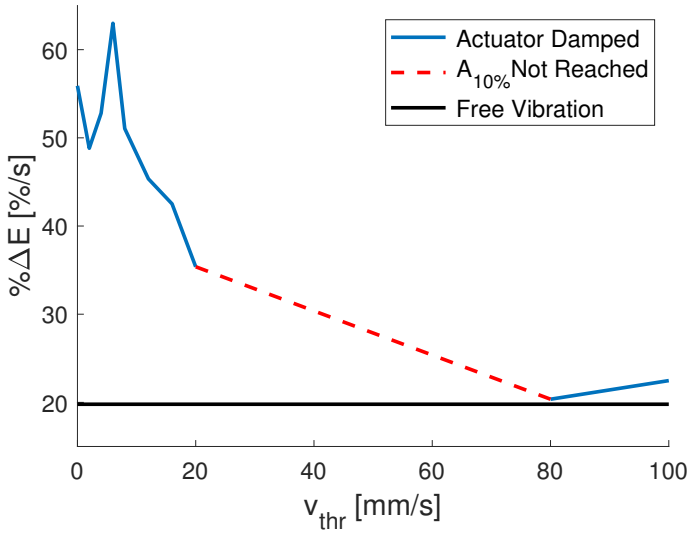

Figure 4.4: Average percentage of energy damped out for selected values for v_{thr} for the cantilever beam of $L = 50cm$.

Figure 4.3 shows the beam vibrating freely, compared to the best damping result for the VT algorithm which was obtained with a threshold value of $v_{thr} = 6mm/s$. 90% reduction in amplitude was obtained in $1.57s$ for the most effective algorithm compared to $5.00s$ for the free vibration case. This is a reduction of more than 65%. The red displacement curve u_a does not reach a state of rest at zero displacement in the logged period. This is because the solenoid continues to be turned on and off after damping out the initial vibrations. Table 4.3 shows the performance of a selection of threshold values in the VT algorithm. For a large set of values, the point of 90% reduction in amplitude was not obtained. Figure 4.4 shows the average percentage energy decay per second in the time period between t_0 and $t_{10\%}$. Lower values of v_{thr} seems to be more efficient than higher values of v_{thr}.

4.3 Cantilever Beam of Length 55 cm

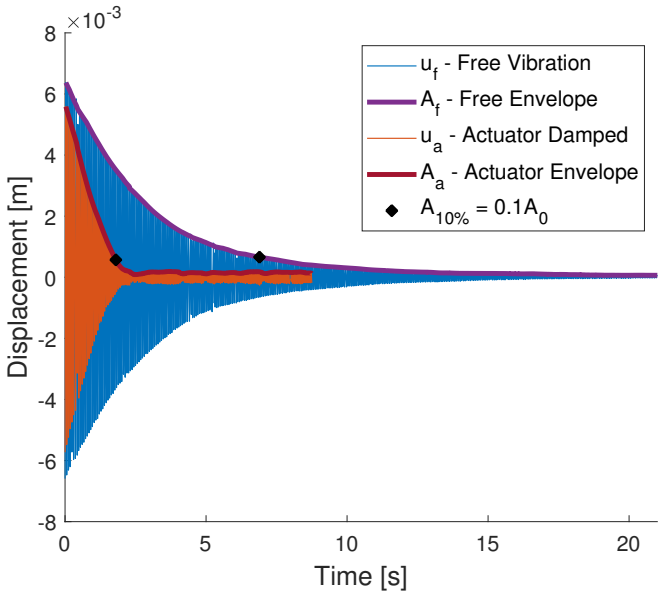

Figure 4.5: Free vibrations and the most effective damping result using the single solenoid configuration with $v_{thr} = 2mm/s$ in the VT algorithm on the cantilever beam of $L = 55cm$.

$v_{thr}[mm/s]$	$A_0[mm]$	$t_{10\%}[s]$	$\xi_{eq}[\%]$	$\Delta E/s[mJ/s]$	$\%\Delta E[\%/s]$
Free	6.59	6.897	0.32	24.55	14.35
0	6.14	1.803	1.23	83.62	54.91
2	5.80	1.801	1.23	73.93	54.97
4	6.04	1.840	1.20	79.00	53.82
6	5.73	1.796	1.23	72.75	55.14
12	6.19	1.966	1.13	76.77	50.37
20	5.97	1.922	1.15	74.21	51.52
30	6.19	2.038	1.08	75.29	48.59
40	6.30	2.236	0.99	71.25	44.28
50	5.83	N/A	N/A	N/A	N/A
60	6.01	N/A	N/A	N/A	N/A
80	6.22	N/A	N/A	N/A	N/A
100	6.16	4.493	0.49	33.97	22.04

Table 4.4: A selection of data obtained on the cantilever beam of $L = 55cm$ using the single solenoid configuration and the VT algorithm.

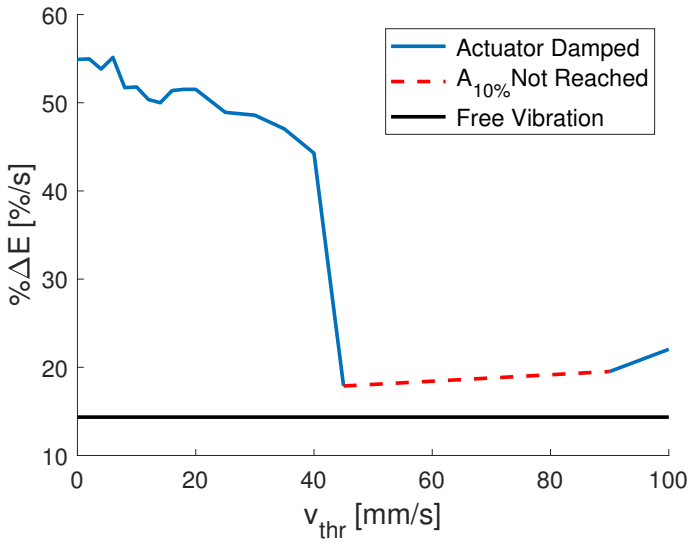

Figure 4.6: Average percentage of energy damped out for a selection of values for v_{thr} in the VT algorithm for the cantilever beam of $L = 55cm$.

Figure 4.5 shows the beam vibrating freely, compared to the best damping result for the VT algorithm which was obtained with a threshold value of $v_{thr} = 2mm/s$. 90% reduction in amplitude was obtained in $1.80s$ for the most effective algorithm compared to $6.90s$ for the free vibration case. This is a reduction of approximately 75%. The red displacement curve u_a does not reach a state of rest at zero displacement in the logged period. This is because the solenoid continues to be turned on and off after damping out the initial vibrations. Table 4.4 shows the performance of a selection of threshold values in the VT algorithm. For a set of values, the point of 90% reduction in amplitude was not obtained. The algorithm seems to be performing well for a large range of threshold values up to approximately $40mm/s$. One then observe a significant drop in performance for higher threshold values. Figure 4.6 shows the average percentage energy decay per second in the time period between t_0 and $t_{10\%}$. Lower values of v_{thr} seems to be more efficient than higher values of v_{thr}.

4.4 Cantilever Beam of Length 60 cm

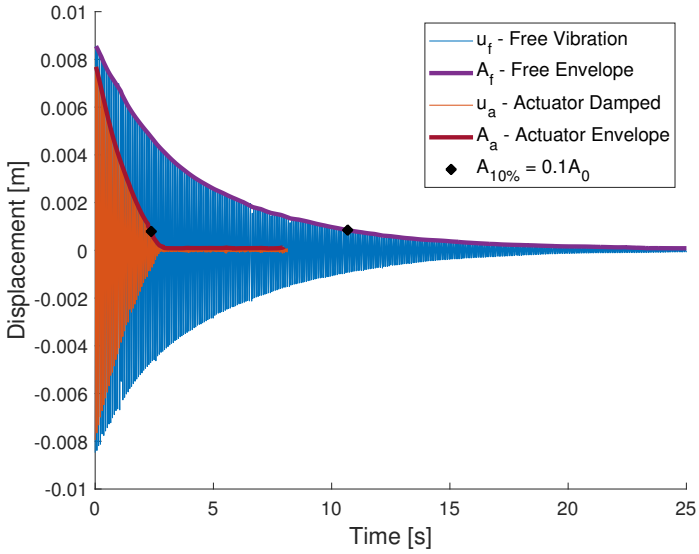

Figure 4.7: Free vibrations and the most effective damping result using the single solenoid configuration with $v_{thr} = 2mm/s$ in the VT algorithm on the cantilever beam of $L = 60cm$.

$v_{thr}[mm/s]$	$A_0[mm]$	$t_{10\%}[s]$	$\xi_{eq}[\%]$	$\Delta E/s[mJ/s]$	$\%\Delta E[\%/s]$
Free	8.48	10.676	0.25	19.94	9.27
0	8.09	2.647	1.01	73.89	37.40
2	7.95	2.372	1.12	79.83	41.74
4	8.57	2.703	0.98	82.54	36.63
6	8.39	2.726	0.97	78.89	36.32
12	8.54	2.726	0.98	80.78	36.32
20	8.58	2.877	0.92	77.39	34.41
30	8.87	2.838	0.94	83.22	34.89
40	8.07	2.839	0.93	70.43	34.88
50	7.25	2.689	0.98	59.67	36.82
60	8.48	2.997	0.88	73.40	33.04
80	8.62	4.012	0.66	56.36	24.68
100	9.02	4.656	0.57	53.35	21.26

Table 4.5: A selection of data obtained on the cantilever beam of $L = 60cm$ using the single solenoid configuration and the VT algorithm.

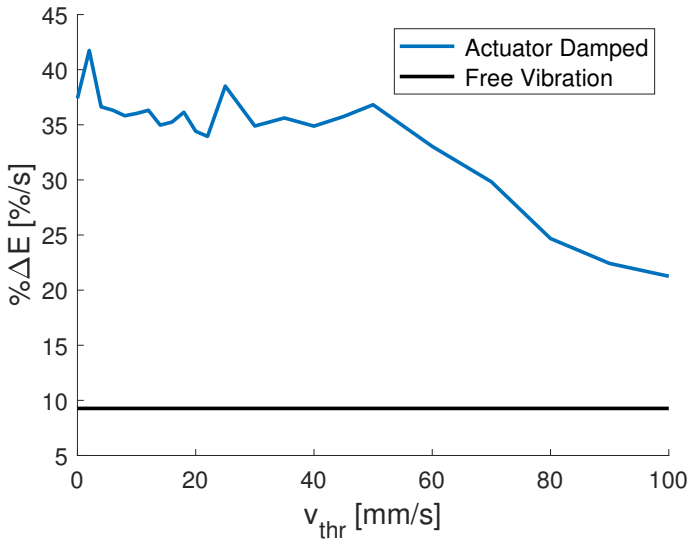

Figure 4.8: Average percentage of energy damped out for a selection of values for v_{thr} in the VT algorithm for the cantilever beam of $L = 60cm$.

Figure 4.7 shows the beam vibrating freely, compared to the best damping result for the VT algorithm which was obtained with a threshold value of $v_{thr} = 2mm/s$. 90% reduction in amplitude was obtained in $2.37s$ for the most effective algorithm compared to $10.68s$ for the free vibration case. This is a reduction of more than 75%. Table 4.5 shows the performance of a selection of threshold values in the VT algorithm. 90% reduction in amplitude were obtained for all threshold values tested. Figure 4.8 shows the average percentage energy decay per second in the time period between t_0 and $t_{10\%}$. Lower values of v_{thr} seems to be more efficient than higher values of v_{thr}.

4.5 Fixed-Ends Beam of Length 125 cm

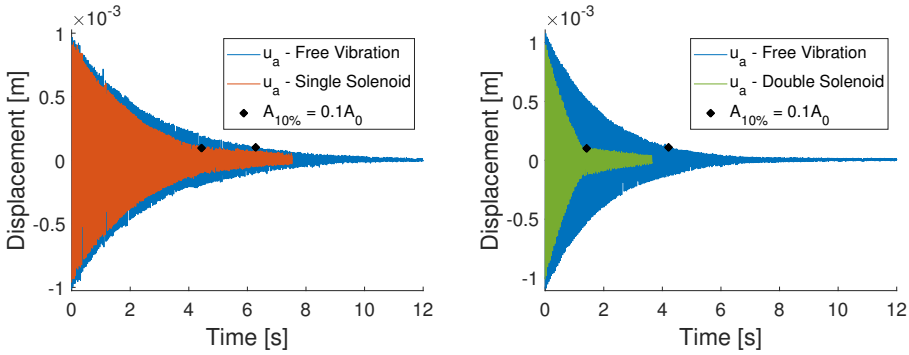

(a) Single solenoid with $d_{thr} = 0.1mm$. **(b)** Double solenoid with $d_{thr} = 0.2mm$.

Figure 4.9: Comparison between the system in free vibration and the best damping result for the single(a) and double(b) solenoid configuration with the VDT algorithm at the fixed-ends beam of length $L = 125cm$. The free vibration tests were carried out with the current solenoid mounted on the rig, but turned off.

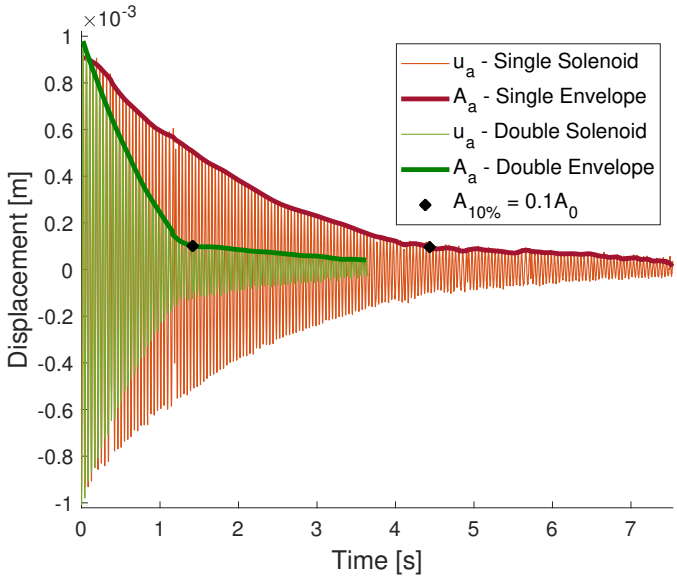

Figure 4.10: Comparison between the best damping result for the single and double solenoid configuration at the fixed-ends beam of length $L = 125cm$.

Config.	d_{thr}	A_0	$t_{10\%}[s]$	$\xi_{eq}[\%]$	$\Delta E/s[mJ/s]$	$\%\Delta E[\%/s]$
Single	Free	1.02	6.291	0.24	3.10	15.74
Single	0.1	0.96	4.436	0.35	3.93	22.32
Double	Free	1.10	4.200	0.37	5.17	23.57
Double	0.2	1.01	1.385	1.11	13.82	71.48

Table 4.6: Damping data for the fixed-ends beam of length $L = 125cm$ for the single and double solenoid configuration. A_0 and d_{thr} are presented in mm.

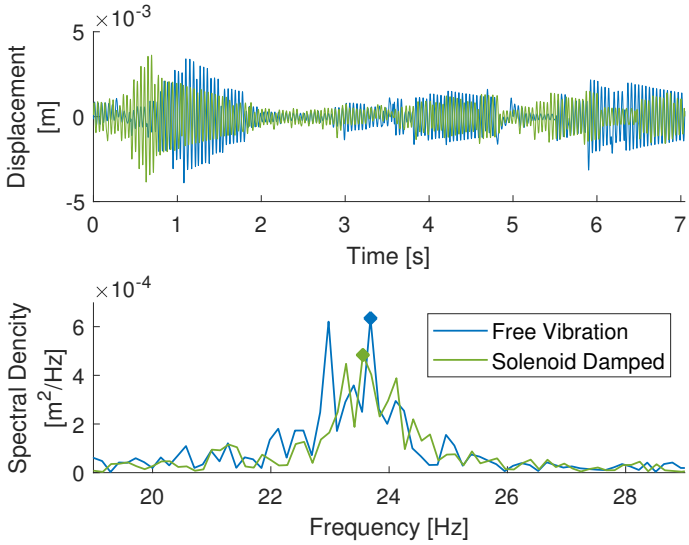

Figure 4.11: FFT analysis of the fixed-ends beam of $L = 125cm$, in undamped vibration and damped by the best double solenoid algorithm. The beam were exposed to random human induced forces and was therefore not identical between the two experiments.

Figure 4.9 shows the fixed-ends beam of length $L = 125cm$ in free vibration compared to the most efficient damping algorithm for the single(a) and double(b) solenoid configuration. The free vibration results of Figure 4.9a and 4.9b are different because the experiments were carried out with the different solenoid configurations mounted on the beam, but turned off. Table 4.6 shows the free vibration experiments compared to the damped experiments. The tests show a significantly better result for the double solenoid configuration, with a 90% reduction in amplitude obtained after $t_{10\%} = 1.39s$, compared to $t_{10\%} = 4.44s$ for the single solenoid configuration. Figure 4.11 shows the FFT analysis for random induced force with the beam in free vibration and the beam damped by the best algorithm with the double solenoid configuration. The plot shows that the damper reduced the maximum value of the spectral density and shift this maximum value to a lower frequency. The improvement is however considered to be small. It is important to emphasize

that the latter experiments were carried out with human induced force. The forces induced on the systems were tried to be similar between the different experiments, but these tests include high uncertainty in the input force.

4.6 Fixed-Ends Beam of Length 145 cm

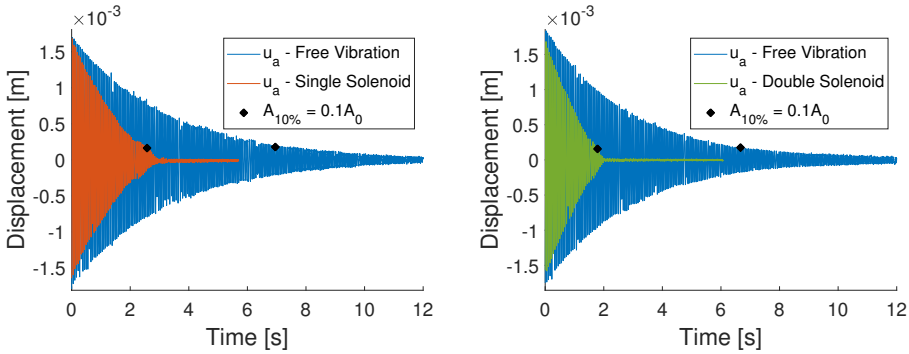

(a) Single solenoid with $d_{thr} = 0.05mm$. **(b)** Double solenoid with $d_{thr} = 0.1mm$.

Figure 4.12: Comparison between the system in free vibration and the best damping result for the single(a) and double(b) solenoid configuration with the VDT algorithm at the fixed-ends beam of length $L = 145cm$. The free vibration tests were carried out with the current solenoid mounted on the rig, but turned off.

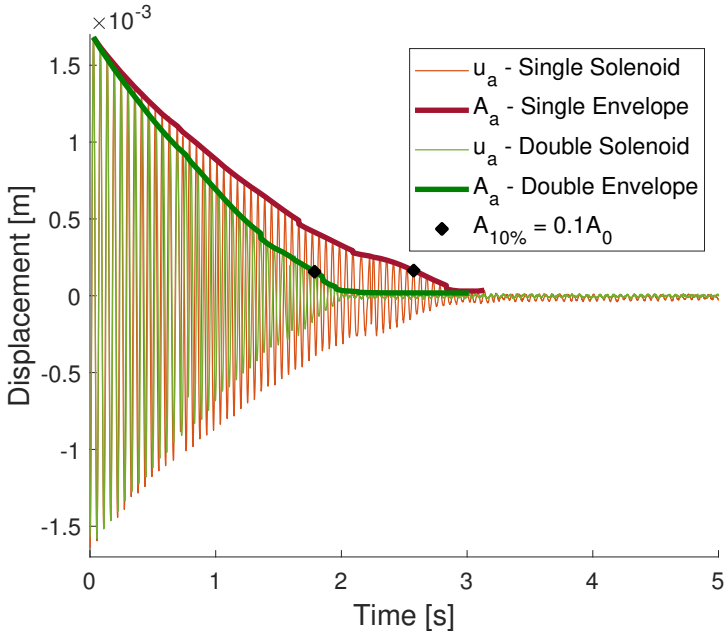

Figure 4.13: Comparison between the best damping result for the single and double solenoid configuration at the fixed-ends beam of length $L = 145cm$.

Config.	d_{thr}	A_0	$t_{10\%}[s]$	$\xi_{eq}[\%]$	$\Delta E/s[mJ/s]$	$\%\Delta E[\%/s]$
Single	Free	1.79	7.194	0.28	5.69	13.76
Single	0.05	1.64	2.580	0.77	13.77	38.37
Double	Free	1.75	6.668	0.30	5.77	14.85
Double	0.1	1.76	1.799	1.12	22.18	55.04

Table 4.7: Damping data for the fixed-ends beam of length $L = 145cm$ for the single and double solenoid configuration. A_0 and d_{thr} are presented in mm.

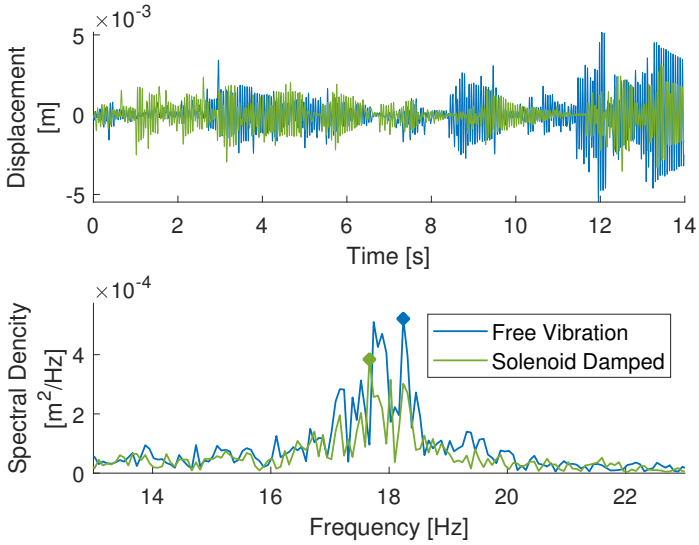

Figure 4.14: FFT analysis of the fixed-ends beam of $L = 145cm$, in undamped vibration and damped by the best double solenoid algorithm. The beam were exposed to random human induced forces and was not identical between the two experiments.

Figure 4.12 shows the fixed-ends beam of length $L = 145cm$ in free vibration compared to the most efficient damping algorithm for the single(a) and double(b) solenoid configuration. The free vibration results of Figure 4.12a and 4.12b are different because the experiments were carried out with the different solenoid configurations mounted on the beam, but turned off. Table 4.7 shows the free vibration experiments compared to the damped experiments. The tests show a better result for the double solenoid configuration, with a 90% reduction in amplitude obtained after $t_{10\%} = 1.80s$, compared to $t_{10\%} = 2.58s$ for the single solenoid configuration. Figure 4.14 shows the FFT analysis for random induced force with the beam in free vibration and the beam damped by the best algorithm with the double solenoid configuration. The plot shows that the damper reduced the maximum value of the spectral density and shift this maximum value to a lower frequency. In this case, the improvement is also considered to be small.

4.7 Fixed-Ends Beam of Length 165 cm

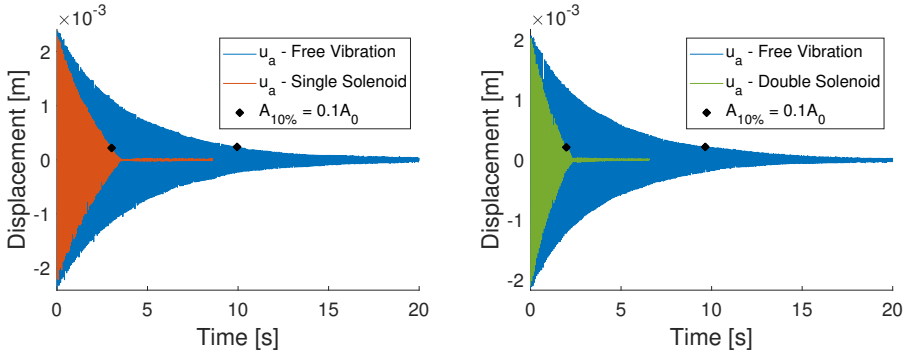

(a) Single solenoid with $d_{thr} = 0.02mm$. **(b)** Double solenoid with $d_{thr} = 0.04mm$.

Figure 4.15: Comparison between the system in free vibration and the best damping result for the single(a) and double(b) solenoid configuration with the VDT algorithm at the fixed-ends beam of length $L = 165cm$. The free vibration tests were carried out with the current solenoid mounted on the rig, but turned off.

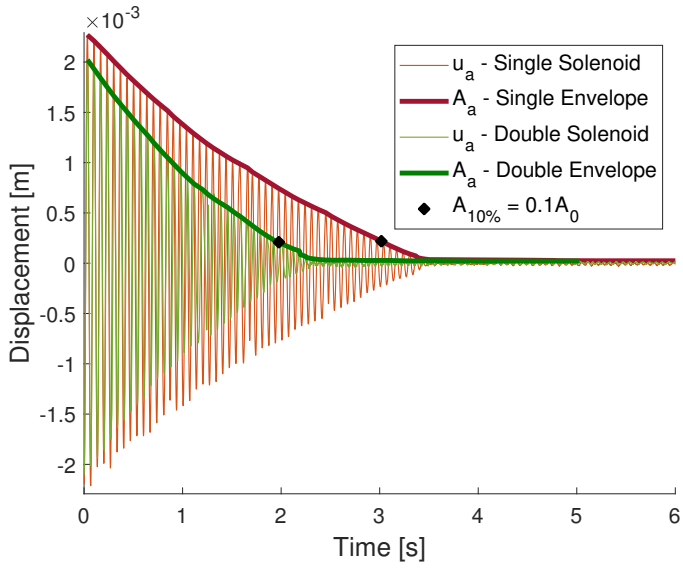

Figure 4.16: Comparison between the best damping result for the single and double solenoid configuration at the fixed-ends beam of length $L = 165cm$.

Config.	d_{thr}	A_0	$t_{10\%}[s]$	$\xi_{eq}[\%]$	$\Delta E/s[mJ/s]$	$\%\Delta E[\%/s]$
Single	Free	2.38	9.947	0.25	5.56	9.95
Single	0.02	2.19	3.020	0.81	15.82	32.78
Double	Free	2.15	9.652	0.26	4.57	10.26
Double	0.04	2.10	1.961	1.26	21.73	50.49

Table 4.8: Damping data for the fixed-ends beam of length $L = 165cm$ for the single and double solenoid configuration. A_0 and d_{thr} are presented in mm.

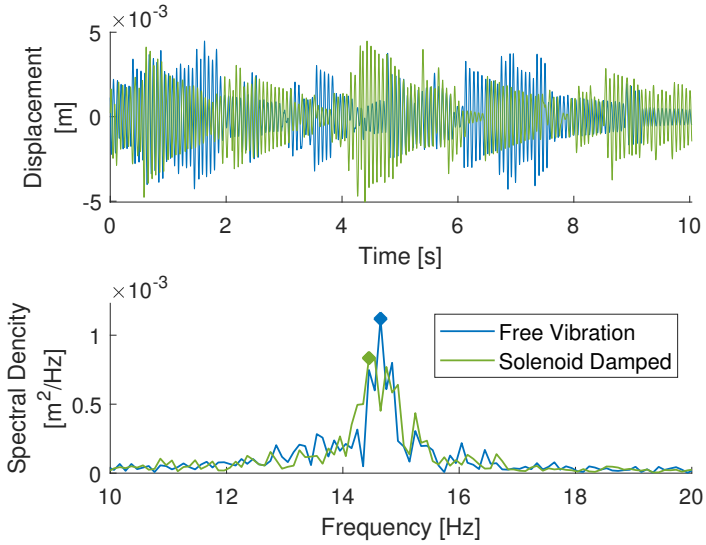

Figure 4.17: FFT analysis of the fixed-ends beam of $L = 165cm$, in undamped vibration and damped by the best double solenoid algorithm. The beam were exposed to random human induced forces and was not identical between the two experiments.

Figure 4.15 shows the fixed-ends beam of length $L = 165cm$ in free vibration compared to the most efficient damping algorithm for the single(a) and double(b) solenoid configuration. The free vibration results of Figure 4.15a and 4.15b are different because the experiments were carried out with the different solenoid configurations mounted on the beam, but turned off. Table 4.8 shows the free vibration experiments compared to the damped experiments. The tests show a better result for the double solenoid configuration, with a 90% reduction in amplitude obtained after $t_{10\%} = 1.96s$, compared to $t_{10\%} = 3.02s$ for the single solenoid configuration. Figure 4.14 shows the FFT analysis for random induced force with the beam in free vibration and the beam damped by the best algorithm with the double solenoid configuration. The plot shows that the damper reduced the maximum value of the spectral density and shift this maximum value to a lower frequency. The improvements shown in the spectral density plot is again considered to be small.

Chapter 5

Discussion

5.1 Discussion of Experiments

The majority of the experiments in this study were carried out with motion induced by an initial displacement. This is different from the conditions of the test tunnel where wind sets the construction into motion. It is reason to believe that the bridge model motions in the wind tunnel will be more varying and random than the test rig. This requires the opportunity to vary the amount of force to put in the system through the actuator to damp out the vibrations. A solenoid with a given force curve may therefore perform better in an experiment where the motion is induced by an initial displacement than by a continuous random force.

5.1.1 Experimental Results

It is evident from the results that low threshold values give a better damping performance than high threshold values in the VT algorithm. This may be explained by studying the time the solenoid piston uses from off-state to on-state and from on-state to off-state. These values proved to be $t_{ON} = 21ms$ and $t_{OFF} = 25ms$, respectively, when the solenoid was placed on solid ground. The piston will most likely use an even longer time when placed on a rig. This is due to the forces from the vibrating beam acting on the solenoid, and hence the electromagnetic coil will have to work harder to accelerate the piston in the same direction as the velocity of the beam. After the solenoid is set into state changing action, two things may cause it to stop:

- The piston reaches its maximum or minimum stroke.
- The piston reaches a threshold value which changes the state of the solenoid.

The highest beam frequency tested was approximately $25Hz$, which gives a period of $T = 0.04s$ and half a period of $T/2 = 0.02s$. This means that the solenoid piston travel for this frequency will be terminated by reaching a new threshold value, since the time

between two threshold values (T/2) are smaller than the solenoid's travel time (t_{ON} and t_{OFF}) between states. Figure 5.1 illustrates one cycle for the beam vibrating at $25Hz$ and of what sections of the period the solenoid will act with threshold values of $v_{thr} = 0$ and $v_{thr} = 100$.

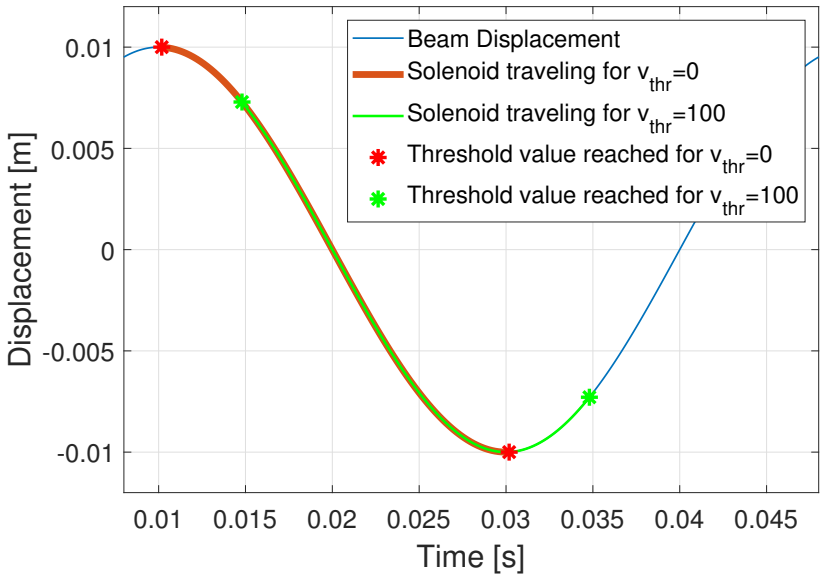

Figure 5.1: Illustration of when the solenoid piston travels between states.

The beam reaches its maximum displacement and obtains zero velocity. This means that the piston of the solenoid will be turned on and start to contract when the threshold value is set to $v_{thr} = 0$. Some time later, the beam will reach a velocity of $100mm/s$, and the solenoid would have been turned on if the threshold value was set to $v_{thr} = 100mm/s$. When the beam reaches its minimum position, the velocity is zero again, and for $v_{thr} = 0$ - the solenoid will be turned off and the piston will start moving in the opposite direction. This action will be delayed when $v_{thr} = 100mm/s$, and in the period $0.03 - 0.035s$, the solenoid will induce a force in the same direction as the beam velocity, thus contributing to excitation, rather than damping. This is relevant when half of the oscillation period is smaller than the traveling time of the solenoid, which happens for higher frequencies. This may explain why a VT algorithm performs worse for higher threshold values, and that this effect is stronger for high frequent beams. This may also explain why the double solenoid configuration performs better than the single solenoid configuration. The piston uses a shorter time when traveling from off-state to on-state than the opposite way around, but for the double solenoid configuration, the solenoids are able to have equal travel time in both directions. This increases the ability for the damper to induce forces within the appropriate time window. The main reason that the double solenoid configuration performs better seems however to be that higher force may be induced to the system in both directions. The force curve from the damper will in this case be described by a graph close to Figure

3.2 in both directions. This obviously gives a higher total force to damp out vibrations than the case where the force graph is described by Figure 3.2 in one direction and Figure 3.3 in the other direction.

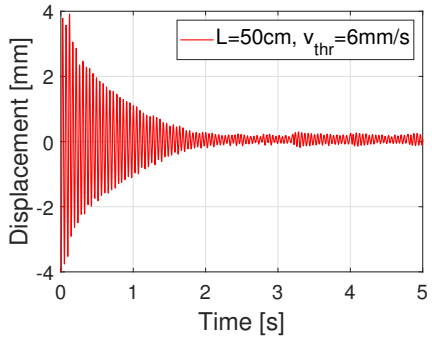

(a) Cantilever, $L = 50cm$, VT algorithm.

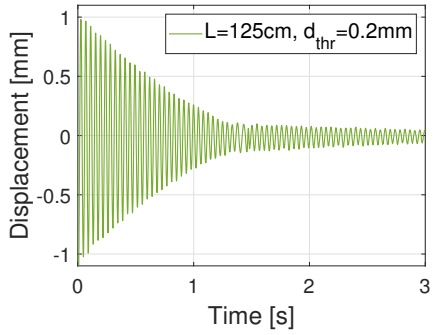

(b) Fixed ends, $L = 125cm$, VDT algorithm.

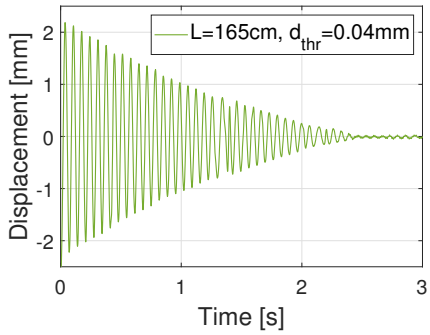

(c) Fixed ends, $L = 165cm$, VDT algorithm.

Figure 5.2: Selection of beam displacement plots for different damping applications to explain pros and cons with the VT and VDT algorithm. The red and green graphs indicate single and double solenoid configuration, respectively. For the VDT algorithm, v_{thr} was set to zero.

Figure 5.2a shows the single solenoid configuration on the cantilever beam of $L = 50cm$ with $v_{thr} = 6mm/s$ in the velocity threshold algorithm, and is a good example on a common problem encountered when using the VT algorithm. The motion is effectively damped the first two seconds, but when it is suppose to stop moving at zero displacement, the solenoid continues to act due to the low velocity threshold. This will excite the beam into new motion and the threshold values will be exceeded again and again. This was as explained in Chapter 3 the reason for introducing the VDT algorithm. Introducing the displacement threshold, d_{thr}, at the right value was important for improved damper function. Figure 5.2b shows the fixed-ends beam of $L = 125cm$, where the displacement threshold by mistake was set too high. The damper works effectively to a point between 1 and 2 seconds before it is turned off too early and the natural damping of the beam takes over. Figure 5.2c shows an example where v_{thr} is set correctly. The test of Figure 5.2b did

however prove to be very effective with the measurements presented in this study, since a displacement amplitude at 10% of the initial amplitude was achieved right around the point where the solenoid was turned off. This indicates that the quantification method of measuring energy dissipation until an amplitude 10% of the initial amplitude have a weakness, because no data after this point is being analyzed.

5.2 Discussion of MATLAB Simulation

As the results show, solenoids may in some cases be used with an active damping algorithm and give adequate results. However, a solenoid has the obvious limitation that it only has two states and that it either acts with full force or it exerts no force at all. This gives motivation to test more advanced actuators, for example a voice coil actuator. A VCA may exert any force lower than its maximum capability and should therefore damp vibrations at least as good, and likely a lot better than a solenoid. VCAs are expensive, more advanced and hence requires more resources to use. As was presented in Section 3.1, a MATLAB simulation was made to simulate the bridge response when damped by both a solenoid and by a VCA. Before using the simulation to predict the performance of a voice coil actuator, it is interesting to compare how the simulation predicts the use of solenoid as active damper to the experimental results of Chapter 4.

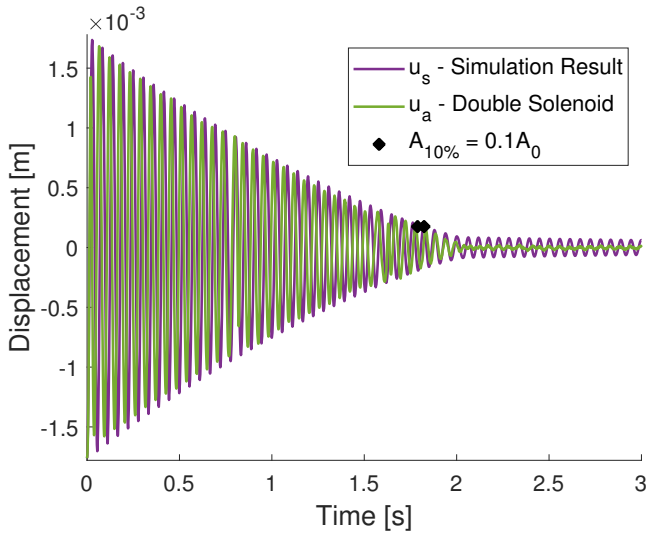

Figure 5.3: Comparison between the results obtained from the initial displacement experiment on the fixed-ends beam of length $145cm$ and the simulation with input $A_0 = 1.76mm$, $f = 18.11Hz$ and $\xi = 0.003$, which were the values obtained for the fixed-ends beam with $L = 145cm$.

Figure 5.3 compares the results from the experiment carried out on the fixed-ends beam of length $145cm$, damped by the double solenoid configuration - to the results from the simulation using the natural frequency, damping ratio and initial displacement as obtained

from that particular experiment. As can be seen, the results are very similar. The point at witch 90% of the amplitude is damped out is almost exactly the same. However, once this point is reached, the results differ. Where the amplitude of the real beam continues to decrease to the point where there is no movement, the simulation results keep oscillating. The simulation does indeed account for the damping ratio of $\xi = 0.003$, but what it does not account for is the fact that the solenoid may still damp out vibrations when turned off. When the solenoid is off, the piston is still able to move, held only in place by the spring and may therefore contribute with some damping. Since the purpose of this simulation is to predict how well an active damper performs, this effect was not included in the simulation.

Config.	d_{thr}	A_0	$t_{10\%}[s]$	$\xi_{eq}[\%]$	$\Delta E/s[mJ/s]$	$\%\Delta E[\%/s]$
Real	0.1	1.76	1.799	1.12	22.18	55.04
Sim.	0.1	1.76	1.833	1.11	23.06	54.03

Table 5.1: Damping data as obtained from the experiment on the fixed ends beam of $L = 145cm$ compared with the damping data predicted by the simulation.

Table 5.1 shows how close the damping data obtained from the simulation are to the data obtained from the experiment. The simulation gives a slightly lower damping than the results from the experiment. However, the simulation is considered to approximate the behaviour of the solenoid and how it affects the beam quite well.

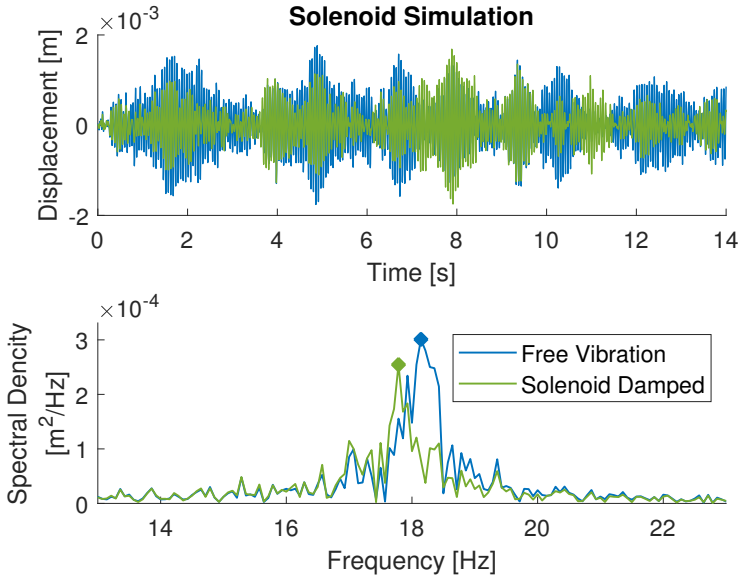

Figure 5.4: Simulation using a random load with zero mean on a system with ω and ξ as obtained from the fixed-ends beam of $L = 145cm$. A_0 was set to 0.

Figure 5.4 presents the simulation results when the same beam analysed in Figure 5.3 is subjected to a random force. This random force was stored as an array so when simulating the response of the beam with no active damper, it would be subjected to the exact same randomly generated force as when simulating the response when damped by the double solenoid configuration. This simulation was made to approximate the conditions when the beam was subjected to a random load as presented in Figure 4.14 in Chapter 4. Considering that the experiment was carried out with a human induced force and the force used in the simulation was generated by a random number generator in MATLAB, the results from the experiment and the simulation should be compared with caution. With that being said, Figure 5.4 and Figure 4.14 from Chapter 4 both show that the solenoid damps the vibrations to some extent. Furthermore, the prominence of the peak corresponding to the natural frequency of the system is reduced and shifted slightly to the left, meaning the natural frequency is lower when the system is damped by an active damper. The similarities between the two figures indicate that the simulation is able to predict the impact the double solenoid configuration has on the fixed-ends beam when subjected to a random load.

The fact that the solenoid has limited damping abilities motivates the use of more advanced actuators, such as voice coil actuators.

$\boldsymbol{Range[mm]}$	$\boldsymbol{Total\ mass[g]}$	$\boldsymbol{Piston\ mass[g]}$	$\boldsymbol{F_{max}[N]}$
6.36	127	17.7	15.57

Table 5.2: Specifications of the Bei Kimco LAS13-18 VCA used in the simulation.

In Table 5.2, some of the specifications of the actuator used in the simulation is presented. The data is collected from the datasheet of the actuator Bei Kimco LAS13-18 [4]. This actuator has a maximum force which far exceeds that of the solenoids used in the experiments. Furthermore, it is not limited to an on or off state, meaning it can be controlled with varying piston acceleration. These properties makes it suitable to use with the Linear Negative Feedback control algorithm as presented in Section 2.5.1. This algorithm may use the structure's position, velocity and acceleration to determine the force the actuator should impose on the structure, in order to damp the vibrations in the most efficient manner. However, by examining the equations in Section 2.5.1, it is suggested that k_d and k_a both are set to zero, leaving k_v as the only non-zero coefficient. This yields the Direct Velocity Feedback (DVF) algorithm as the most effective algorithm to damp the vibrations of an oscillating system.

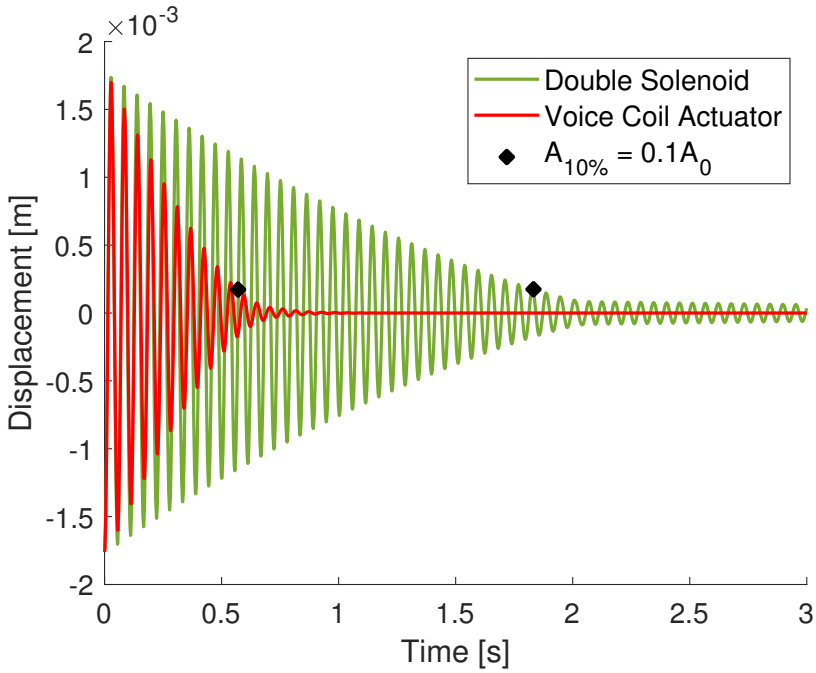

Figure 5.5: Simulation result of the damping by the double solenoid compared to the damping by a voice coil actuator with an initial displacement of $A_0 = 1.76mm$ on a fixed-ends beam of $L = 145cm$. For the double solenoid configuration, the VDT algorithm was used with the values $v_{thr} = 0$ and $d_{thr} = 0.1mm$. The VCA was used with the DVF algorithm with $k_v = 2500s^{-1}$.

Config.	$\boldsymbol{d_{thr}/k_v}$	$\boldsymbol{A_0}$	$\boldsymbol{t_{10\%}[s]}$	$\boldsymbol{\xi_{eq}[\%]}$	$\boldsymbol{\Delta E/s[mJ/s]}$	$\boldsymbol{\%\Delta E[\%/s]}$
DSC	$d_{thr} = 0.1$	1.76	1.833	1.11	23.06	54.03
VCA	$k_v = 2500$	1.76	0.569	3.57	75.83	173.98

Table 5.3: Data obtained from the simulations of Figure 5.5. d_{thr} is given in the unit mm and k_v in s^{-1}. DSC denotes the double solenoid configuration.

By studying Figure 5.5, it is obvious that the VCA is much more efficient in terms of damping vibrations compared to the double solenoid configuration. Looking at Table 5.3, one observe that the energy dissipates more than three times faster when using the VCA compared to the use of solenoids. In addition, the VCA is able to damp the vibrations to the point where the structure is at complete rest, whereas the solenoid is forced to stop to prevent it from exiting the vibrations rather than damping them out. This is as expected, considering that both the VCA and the DVF algorithm are a lot more sophisticated than the double solenoid configuration and the VDT algorithm.

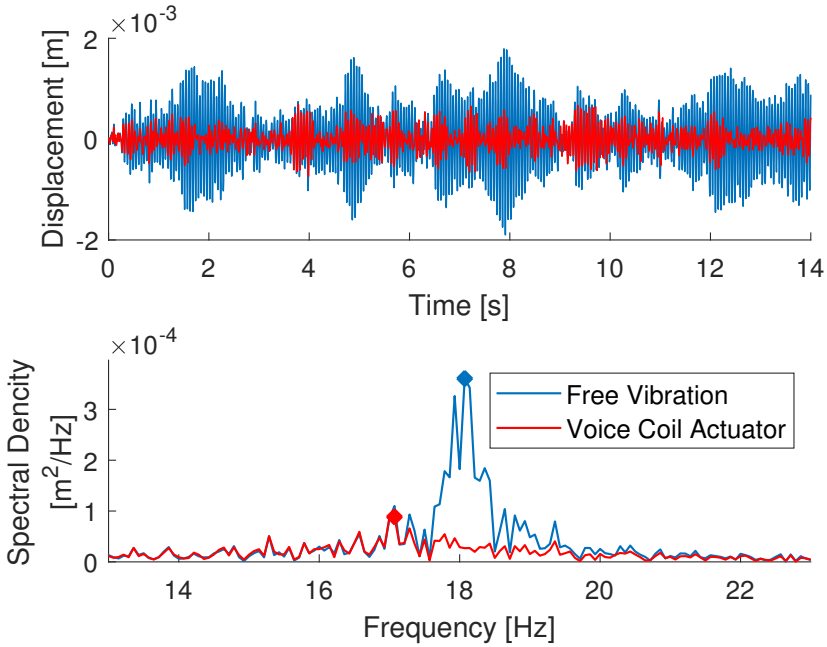

Figure 5.6: Simulation result of a VCA damping vibrations due to a random load for a fixed-ends beam of length $L = 145cm$. The case of free vibration is included.

Figure 5.6 shows the same beam as in Figure 5.5, this time induced by a random force, in both free vibration and with VCA as active damper. The VCA is capable of significantly reducing the structure response. By looking at the spectral density, the prominence of the peak corresponding to the natural frequency is significantly smaller when the structure is damped by the VCA. The natural frequency of the system has also reduced by approximately $1Hz$. This reduction is also expected, based on the theory described in Section 2.5.1.

The parameters k_d, k_v and k_a from the Linear Negative Feedback algorithm discussed in Section 2.5.1, are scalar numbers that often are obtained through experimental testing. These parameters serve as weights so the algorithm can balance the effect of position, velocity and acceleration differently. The Linear Negative Feedback algorithm yields Equation 2.26 and Equation 2.27 which are both restated here:

$$\omega_{LNF} = \sqrt{\frac{k + k_d}{m + k_a}} \tag{5.1}$$

$$\xi_{LNF} = \frac{1}{\omega_{eq}} \frac{c + k_v}{2(m + k_a)} \tag{5.2}$$

In Equation 5.2, one may observe that increasing k_v, also increases ξ_{LNF}. Furthermore, if k_a is assigned a negative value, this will also increase the value of ξ_{LNF}. This gives motivation to test a positive value for k_v, in combination with a negative value of k_a.

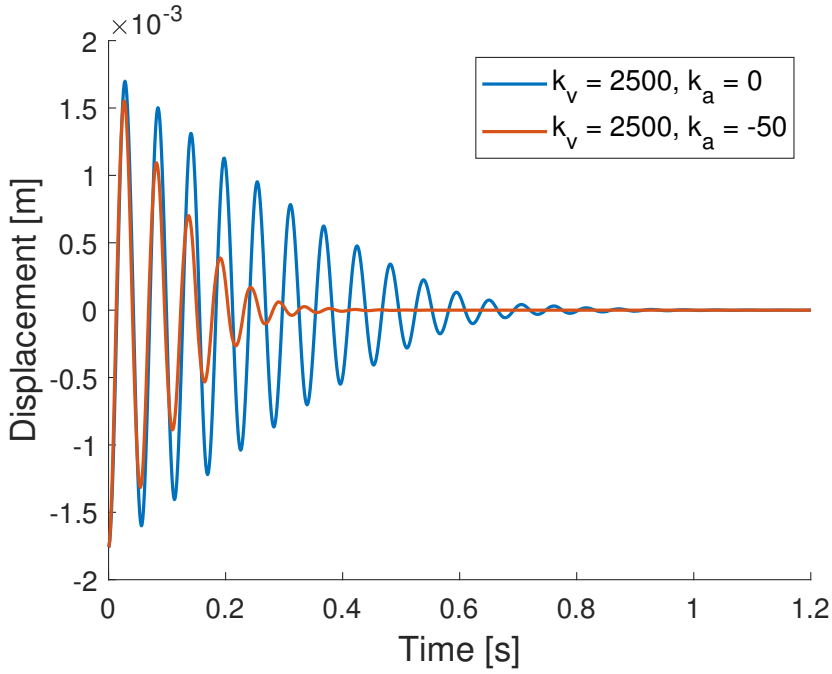

Figure 5.7: The effect of using only k_v compared to combining the use of k_v and k_a in the LNF algorithm with a VCA as active damper, on a fixed-ends beam of $L = 145cm$.

Config.	k_v	k_a	A_0	$t_{10\%}[s]$	$\xi_{eq}[\%]$	$\Delta E/s[mJ/s]$	$\%\Delta E[\%/s]$
k_v *only*	2500	0	1.76	0.569	3.57	75.83	173.98
k_v *and* k_a	2500	-50	1.76	0.409	4.96	105.57	242.20

Table 5.4: Data obtained when using only k_v, compared to optimized values of k_v and k_a in the LNF algorithm with a VCA as active damper, on a fixed-ends beam of $L = 145cm$.

Figure 5.7 and Table 5.4 both show that assigning a negative value for k_a improves the performance of the VCA when damping vibrations caused by an initial displacement. From Figure 5.8, it is however evident that the prominence of the peak corresponding to the natural frequency in the spectral density plot increases when $k_a < 0$. The same plot also reveal that the natural frequency increases, which is expected from Equation 5.1.

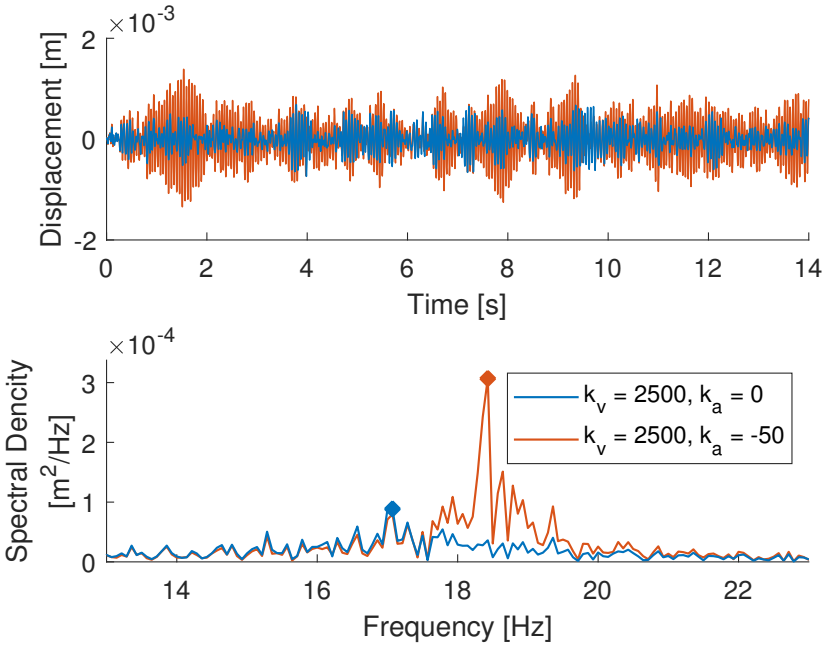

Figure 5.8: The effect in spectral density when using only k_v compared to combining the use of k_v and k_a when damping vibration caused by a random force, on a fixed-ends beam of $L = 145cm$.

The results from the simulation show that a voice coil actuator performs far better than a solenoid, in terms of damping the system when the oscillations are exited by both an initial displacement and random forces. The simulation is able to predict how the structure responds when damped by a solenoid, and might therefore serve as an indicator of how one can expect a similar structure will behave when subjected to a VCA damper. The simulation could produce results that are better than the results one would obtain in a real experiment using a VCA or even faulty results due to simplifications and approximations made when creating the simulation. If treated with caution, the simulation may however serve as an effective way to test various algorithms, experiment with different values for k_d, k_v and k_a and test actuators before purchasing expensive equipment or performing time consuming experiments in a laboratory.

5.3 Suggestions for Further Work

As previously discussed, it is reason to believe that a VCA would be better suited for damping out wind induced vibrations, given the opportunity to vary the amount of force applied from the actuator. This also makes it possible to control the system with the direct velocity feedback algorithm discussed in Chapter 2. Regrettably, VCA along with the Developers Kit was available too late in this project in order to be tested in the laboratory. A suggestion on how to set up a VCA active damping application with equipment now available at the Department of Structural Engineering is therefore presented. The following list summarizes necessary equipment and their purposes.

- A Kistler accelerometer may be mounted on the bridge to measure the vibration.
- If a direct velocity feedback is to be used, the acceleration signal needs to be post-processed by integration and filtering before passed into the control. These calculations must be carried out in a short period of time to prevent critical delay time between a measured signal and the desired action is carried out. A CompactRIO contains a FPGA (field programmable gate array), well suited for fast calculations. The CompactRIO may be programmed with the aid of LabVIEW to perform the desired integration and filtering in a short period of time before the analog signal is passed on to the control.
- *VCA Developer's kit* from Bei Kimco contains a voice coil actuator and a Pluto Motion Control Digital Servo Drive. The servo drive may be used as the controller by passing in the filtered analog signal from the CompactRIO and give output for action to the VCA. The control algorithm may be programmed with the aid of the software MotionLAB.

Figure 5.9 illustrates the setup explained above.

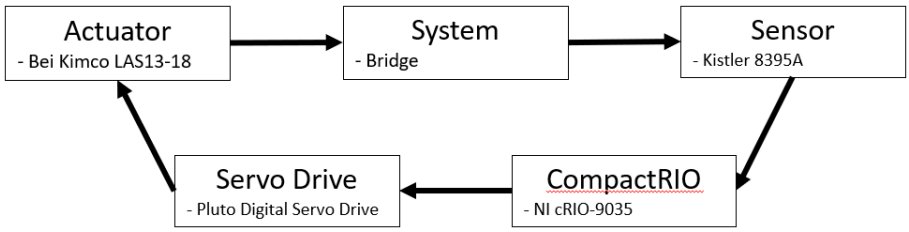

Figure 5.9: Illustration of a active damping application with accelerometer and voice coil actuator.

5.3.1 CompactRIO for Signal Processing

CompactRIO is a real-time industrial controller system developed by National Instruments and consists of both a microcontroller and a programmable FPGA to carry out signal processing. A FPGA is a data chip containing numerous logic blocks and configurable connections between them, which makes it possible to program several algorithms to be executed simultaneously. This is different from a regular CPU which carries out commands

sequentially. This makes the CompactRIO ideal to process data in a limited amount of time. National Instruments offers several models of the CompactRIO, the NI cRIO-9035 was used for research in this project. The CompactRIO model has USB ports which makes it possible to save logged data directly to a memory stick for post-processing. By adding modules to the device, one may process input and output signals. In this project, the analog input module NI 9234, and analog output module NI 9263 were used. The fundamental specifications of these modules can be obtained in Table 5.5.

-	**NI 9234**	**NI 9263**
Input/Output	Input	Output
Nr. of Channels	4	4
Voltage Range	$\pm$5V	$\pm$10V
Connection	Coaxial BNC	Screw/Spring Terminal
Max. Data Rate	51.2kS/s	100kS/s

Table 5.5: CompactRIO modules specifications [16] [15].

Both the input and output modules operate with voltage signals. Calibration of sensors is therefore necessary in order to relate the physical property to the correct corresponding voltage value. Figure 5.10 shows the the CompactRIO model with the two analog modules.

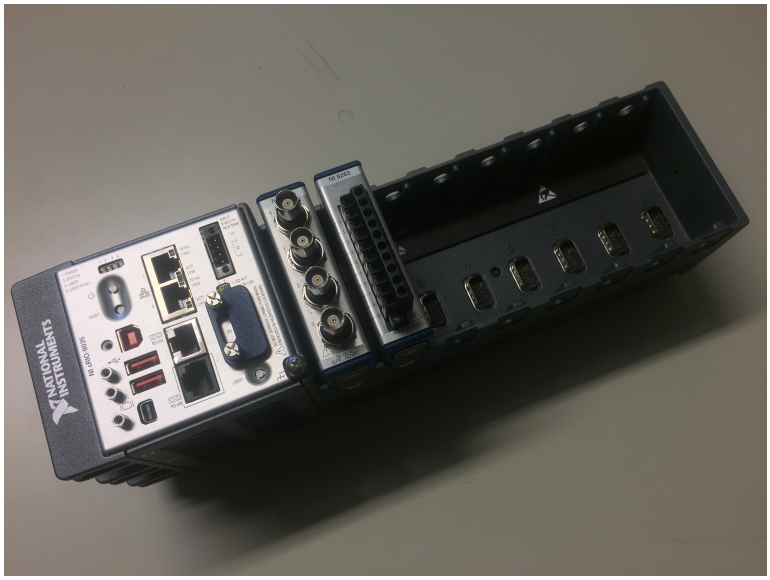

Figure 5.10: National Instruments CompactRIO 9035.

The CompactRIO can be connected to a computer via a WiFi router connected by Ethernet cable to the CompactRIO device. This makes it possible to program the CPU and FPGA of the device and develop a signal processing application based on voltage signals from the

input module. LabVIEW is the software from National Instruments used for this purpose. It uses a graphical block programming interface with a number of pre-configured function blocks. This includes everything from basic numeric operations to PID controls, digital philters and data type converters. This makes it simple to develop the desired application and monitoring important parameters in real-time. The FPGA may be used to acquire data from the four channels of the input module through a FPGA FIFO (First-in First-Out). The concept of the FIFO configuration is illustrated in Figure 5.11.

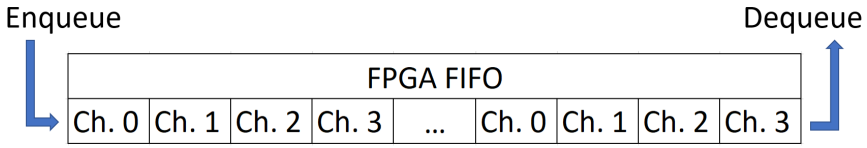

Figure 5.11: Concept of FIFO.

The FIFO may take values of the four channels from the AI module in accordance with the specified sampling frequency. This makes a time efficient data acquiring process.

5.3.2 Servo Drive and VCA as Regulator and Actuator

The *VCA Developer's Kit* from *BEI Kimco* is a set including a Pluto servo drive, a LAS13-18-000A-P01 voice coil actuator and configuration setup in the software MotionLab. With this software, it is possible to program the servo drive to operate the VCA in the desired way, based on an analog input signal or directly from the software on the computer. The specifications of the VCA available may be obtained in Table 5.6. This particular VCA also includes a position sensor which makes it possible to always know where in the coil the piston is placed. This information is highly useful and can identify when the piston for example is positioned at minimum or maximum stroke, thus indicating that no more force may be induced to the system in one particular direction.

-	**LAS13-18-000A-P01**
Peak Force [N]	15.57
Total Stroke [mm]	6.36
Voltage at Peak Force [V]	27.2
Current at Peak Force [A]	1.59
Piston Mass [g]	17.7
Total Mass [g]	127

Table 5.6: Specifications for the voice coil actuator LAS13-18-000A-P01 from BEI Kimco [4].

Figure 5.12 shows the servo drive, the VCA and a to the right, an electrical fuse, preventing current overload to the actuator.

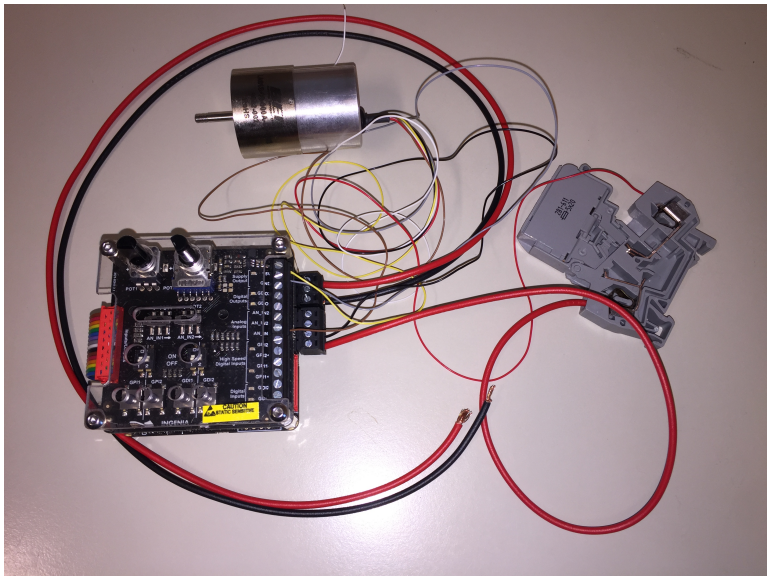

Figure 5.12: Pluto servo drive and LAS13-18-000A-P01 voice coil actuator.

From Table 5.6 it is evident that the VCA is more powerful and may provide a higher force to the system than the solenoid tested in this project. At maximum stroke, the total length of the actuator from bottom to piston tip is $61.6mm$ [4]. This size is small enough to for example be placed inside the section model of the Hardanger Bridge, which have a maximum height of $65mm$ [20]. It would be interesting to further study how the suggested setup works when mounting the VCA inside the bridge deck. Where this project have focused on experiments with an initial system displacement, tests with continuous wind load needs to be further investigated. Experiments are needed to optimize the application and the parameters of the feedback algorithm.

Chapter 6

Conclusion

The experimental and numerical results of this project indicates that solenoids are effective for damping out vibrations in beams caused by an initial displacement. The solenoids used have a maximum output force of only $1.72N$, but are still able to significantly reduce the time it takes for the amplitude of the vibrations to reach 10% of its initial value. Experiments reveal that a double solenoid configuration is more effective than a single solenoid, since the most powerful and fast-responding direction of the traveling piston may be used in both directions. The most effective solenoid algorithm seems to be a velocity-displacement threshold algorithm, where the velocity threshold is set to zero or close to zero, and the displacement threshold is set sufficiently low to ensure that the solenoid stops acting when the vibrations are damped out. These conclusions are based on the results from the experiments and when compared to the simulation results it was confirmed that the MATLAB simulation was very accurate. This Indicates that the project was successful in developing a program that simulates a vibrating single degree of freedom system subjected to different active damping configurations.

Experiments and MATLAB simulation indicates that the solenoids used in this project perform poorly when the system they are mounted on are subjected to random forces. A system subjected to random forces is more relevant to wind tunnel testing than a system set in motion by an initial displacement with no external loads. Voice coil actuators are therefore suggested as actuators in the active damping configuration, since they have the ability to vary the output force subjected to the system. Simulation with the VCA model *Bei Kimco LAS13-18-000A-P0* shows significant reduction in the power spectral density of a system subjected to random forces, compared to the double solenoid configuration. Regrettably, this VCA was not available in time for experimental testing. Future testing with the VCA as active damper - both on the test rig and in the wind tunnel - is therefore necessary to verify that VCAs are better suited as active damping actuators on the bridge section models of the wind tunnel.

Bibliography

[1] Datasheet solentec sd0630 solenoid. https://docs.rs-online.com/c4ff/0900766b815dfd71.pdf. Accessed: 2019-12-13.

[2] Kistler acceleration datasheet. https://www.kistler.com/fileadmin/files/divisions/sensor-technology/test-and-measurement/t-m-_acceleration/900-380a.pdf. Accessed: 2019-12-13.

[3] Research, structural dynamics group, department of structural engineering. https://www.ntnu.edu/kt/research/dynamics/research. Accessed: 2019-12-13.

[4] BEI Kimco. *Datasheet Voice Coil Actuator LAS13-18-000A-P01*, 2013.

[5] R. D. Blevins. *Formulas for Dynamics, Acoustics and Vibrations*. John Wiley & Sons, 2015. ISBN: 9781119038115.

[6] V. L. Boginski, C. W. Commander, P. M. Pardalos, and Y. Ye. *Sensors: Theory, Algorithms, and Applications*. Springer, 2012. ISBN: 978-0-387-88618-3.

[7] J. Connor and S. Laflamme. *Structural Motion Engineering*. Springer, 2014. ISBN: 978-3-319-06280-8.

[8] C. Dincer et al. *Disposable Sensors in Diagnostics, Food, and Environmental Monitoring*. Imperial College London, 2019. DOI: 10.1002/adma.201806739.

[9] P. Gwalani. *Vibration Control Using Tuned Mass Damper*. International Journal of Engineering Research in Mechanical and Civil Engineering, 2017. ISSN: 2456-1290.

[10] F. Haugen. *Basic Dynamics and Control*. TechTeach, 2010. ISBN: 978-82-91748-13-9.

[11] O. C. Hermanrud. *Master Thesis, Active and Passive Damping Systems for Vibration Control of Metal Machining Equipment*. NTNU, 2017.

[12] D. J. Inman. *Vibration with Control*. John Wiley and Sons, 2006. ISBN 0-470-01051-7.

[13] S. G. Kelly. *Mechanical Vibrations Theory and Applications, SI Edition*. Cengage Learning, 2011. ISBN-13: 978-1-4390-6214-2.

[14] Kimco Magnetics Division, BEI Technologies Inc. *Voice Coil Actuators An Applications Guide*.

[15] National Instruments. *Datasheet NI 9234*, 2015.

[16] National Instruments. *Datasheet NI 9263*, 2016.

[17] A. Pavic and P. Reynolds. *Key Results of Modal Testing of the Millennium Bridge, London*. 2002.

[18] A. Preumont. *Vibration Control of Active Structures An Introduction, Fourth Edition*. Springer, 2018. ISBN: 978-3-319-72295-5.

[19] B. Siedziako. *Doctoral Thesis, Modelling of the Self-Excited Forces for Bridge Decks Subjected to Random Motions: An Experimental Study*. NTNU, 2017.

[20] B. Siedziako, O. Øiseth, and A. Rønnquist. *An Enhanced Forced Vibration Rig for Wind Tunnel Testing of Bridge Deck Section Models in Arbitrary Motion*. Journal of Wind Engineering and Industrial Aerodynamics, 2017. DOI: 10.1016/j.jweia.2017.02.011.

[21] A. Sinha. *Vibration of Mechanical Systems*. Cambridge University Press, 2010. ISBN: 978-0-521-51873-4.

[22] S. W. Smith. *The Scientist and Engineer's Guide to Digital Signal Processing, Second Edition*. California Technical Publishing, 1999. ISBN: 0-9660176-7-6.

[23] W. C. Young and R. G. Budynas. *Roark's Formulas for Stress and Strain, Seventh Edition*. McGraw-Hill, 2002. ISBN: 0-07-072542-X.

[24] D. Yurchenko. *Tuned Mass and Parametric Pendulum Dampers under Seismic Vibrations*. 2015. DOI: 10.1007/978-3-642-36197-5-228-1.

Appendix

MATLAB Simulation Code

systSim.m

```
%% System Simulation
%{
$Author: Daniel Harper & Lars Maukon Muren
$Date: 2019/12/01

SYSTSIM:
The purpase of this script us to simulate the responce of a
Cantilever orma Fixed Ends Beam both for free vibrations or
when damped by a Voice Coil Actuator or a Solenoid.

USAGE:
Under the section "Configure Analysis" the analyst may set
desired parameters for the simulation. No other changes
should be necessary.

CALLS:
systSim calls the following functions:
1. getSolenoid(actuatorType,pistonPosition,state); or
   getActuator(actuatorType)
    Depends on simulation configuration,
    returns actuator information.
2. beamData(fn_target, beamType)
    returns information about beam
3. regulator(ddU(i), dU(i), U(i), Ka, Kv, Kd)
    returns the optimal acceleration for the actuator piston
    Note: not in use if the actuator is a solenoid
4. actuator(acc_recomended, ddU_a(i), dU_a(i), U_a(i),...
            dt, actuatorType,dU(i), v_thr);
    Calculates and returns the force and kinetic responce
    of the actuator
5. Newmark_getResponse(U(i), dU(i), ddU(i),...
                       dt, m, c, k, F_act(i) + F_ext(i));
    Calculates the bridge responce based on
    position, velocity, acceleration and external forces
    (i.e from the actuator) for one time increment

The results are plotted at the end of a simulation.
%}

clear all %#ok<CLALL>
close all
```

```
clc
%% Configure Analysis

% Simulation duration in seconds
duration = 3; % seconds

% Sample frequency
FS = 1000; % Sample frequency
    %NOTE: if FS<0, regulator is called every dt

% Load and initial displacement
savedRand = false; % A saved random force vector
randSig = false; % Random signal if true
randAmp = 500; % Amplitude of random signal
wave = false; % Wave load with frequency equal to omega_1
waveAmp = 1; % Amplitude of sinusoidal wave
step = true; % Use an initial displacement
initialDisplacement = -0.00176; % meters

% Structure properties
beamType = "doublefixed"; %"cantiliver" or "doublefixed"
fn_target = 18.17; % Natural frequency of system
xi_target = 0.003; % Damping ratio of the system

% Actuator
actuatorType = "NONE";
    % "SOLENOID_DOUBLE", "LAH13-18-000A-DASH", "NONE"
    % See getActuator or getSolenoid for more
v_thr = 0; % Velocity threshold for solenoid
p_thr = 0.00; % meters position threshold form last periods

% Regulator Variables (Not relevant for solenoids)
Ka = 0;    % weight of structure acceleration
Kv = 2500; % weight of structure velocity
Kd = 0;    % weight of structure displacement

%% Time scope
t_end = duration;% seconds
t_start = 0; % seconds
dt = 0.000001; % seconds, dt=0.000001 is suffisient for fn<40 Hz
t_vec = t_start:dt:t_end;
t = t_start;

%% Get Actuator Mass
if contains(actuatorType,"SOLENOID")
    [m_add, ~, ~, ~, ~, ~] = getSolenoid(actuatorType,...
                                         0,...
                                         "still");
else
    [m_add, ~, ~, ~, ~, ~] = getActuator(actuatorType);
```

```
92  end
93
94  %% System variabels
95  wn = 2*pi*fn_target;
96  [L, b, h, ro, m_beam] = beamData(fn_target, beamType);
97  m_modal = m_beam/2; %mass lumping
98  m = m_modal + m_add;
99  k = m*(2*pi*fn_target)^2;
100 c = xi_target*2*sqrt(k*m);
101
102 %% Prepare Solenoid p_thr vector if VDT algorithm
103 if (contains(actuatorType, "SOLENOID") && p_thr ~= 0)
104     T = 1/fn_target;
105     periodPoints = fix(T/dt)+1;
106     lastPeriod = ones(1,periodPoints)*inf;
107 else
108     lastPeriod = inf;
109 end
110 %% Initial conditions:
111 u0 = 0; % meters
112 du0 = 0; % meters pr second
113 ddu0 = 0; % meters pr second^2
114 u_a0 = 0; % meters
115 du_a0 = 0; % meters pr second
116 ddu_a0 = 0; % meters pr second^2
117 if (step == true)
118     u0 = initialDisplacement;
119 end
120
121 %% Value Vectors
122 U = zeros(1,length(t_vec)); % Beam Displacement
123 dU = zeros(1,length(t_vec)); % Beam Velocity
124 ddU = zeros(1,length(t_vec)); % Beam Acceleration
125 U_a = zeros(1,length(t_vec)); % Actuator Pos. relative to beam
126 dU_a = zeros(1,length(t_vec)); % Actuator Vel. rel. to beam
127 ddU_a = zeros(1,length(t_vec)); % Actuator Acc. rel. to beam
128 F_act = zeros(1,length(t_vec)); % Force from the actuator
129
130
131 %% Initial Conncitions placed in the vectors
132 U(1) = u0;
133 dU(1) = du0;
134 ddU(1) = ddu0;
135 U_a(1) = u_a0;
136 dU_a(1) = du_a0;
137 ddU_a(1) = ddu_a0;
138
139 %% Add External force
140 F_rand_saved = zeros(1,length(t_vec));
141 F_rand = zeros(1,length(t_vec));
```

```
142 F_wave = zeros(1,length(t_vec));
143
144 % Create random force vector
145 if (randSig == true)
146     F_rand = 2*randAmp*ones(...
147         1,length(t_vec)).*rand(1,length(F_rand)) - randAmp;
148 end
149 % Create sine wave with frequency w_n
150 if (wave == true)
151     F_wave = waveAmp*sin(wn.*t_vec);
152 end
153 % Load saved random force vector
154 if (savedRand == true)
155     F_loaded = load("Saved_Random_Force");
156     F_rand_saved = F_loaded.F_rand_saved;
157 end
158 % Add external forces together
159 F_ext = F_wave + F_rand + F_rand_saved(1:length(t_vec));
160
161 %% Perform Simulation
162 sampleLimit = fix(1/(FS*dt));
163 sampleCounter = sampleLimit -1;
164 acc_recomended = 0;
165 if (contains(actuatorType, "SOLENOID") && p_thr ~= 0)
166     lastPeriod(end) = U(1);
167     periodPlace = 1;
168     updatePeriod = true;
169 else
170     updatePeriod = false;
171 end
172 for i = 1:(length(t_vec)-1)
173
174     % Only update actuator FS times pr second
175     if(sampleCounter == sampleLimit || FS < 0)
176         sampleCounter = 0;
177         %Get recommended actuator acceleration
178         acc_recomended = regulator(ddU(i),...
179                                    dU(i),...
180                                    U(i),...
181                                    Ka,...
182                                    Kv,...
183                                    Kd);
184     end
185     sampleCounter = sampleCounter + 1;
186
187     % Get force and responce from actuator
188     [F_a, acc_a, vel_a, pos_a] = actuator(acc_recomended,...
189                                           ddU_a(i),...
190                                           dU_a(i),...
191                                           U_a(i),...
```

```
192                                                 dt,...
193                                                 actuatorType,...
194                                                 dU(i),...
195                                                 v_thr,...
196                                                 p_thr,...
197                                                 max(abs(lastPeriod)));
198
199
200     % Store actuator responce
201     F_act(i+1) = F_a;
202     ddU_a(i+1) = acc_a;
203     dU_a(i+1) = vel_a;
204     U_a(i+1) = pos_a;
205
206     % Calculate bridge response
207     F_ext_tot = F_act(i) + F_ext(i);
208     [U(i+1), dU(i+1), ddU(i+1)] = newmark_getResponse(U(i),...
209                                                       dU(i),...
210                                                       ddU(i),...
211                                                       dt,...
212                                                       m, c, k,...
213                                                       F_ext_tot);
214     %% arrange last period
215     if (updatePeriod)
216         if periodPlace > length(lastPeriod)
217             periodPlace = 1;
218         end
219         lastPeriod(periodPlace) = U(i+1);
220         periodPlace = periodPlace +1;
221     end
222
223 end
224
225 %% Plot Results
226
227 % Plot force from actuator;
228 figure
229 plot(t_vec,F_act)
230 title("Force from the actuator")
231 xlabel("t  [s]")
232 ylabel("F  [N]")
233
234 % Plot Acctuator mass Pos, Vel and Acc
235 figure
236 subplot(3,1,1)
237 plot(t_vec,ddU_a)
238 title("Actuator Response")
239 ylabel("Acc  [m/s^2]")
240 xlabel("t  [s]")
241
```

```
242 subplot(3,1,2)
243 plot(t_vec,dU_a)
244 ylabel("Vel  [m/s]")
245 xlabel("t  [s]")
246
247 subplot(3,1,3)
248 plot(t_vec,U_a)
249 ylabel("Pos  [m]")
250 xlabel("t  [s]")
251
252 % Plot Bridge Pos, Vel and Acc
253 figure
254 subplot(3,1,1)
255 plot(t_vec,ddU)
256 title("Bridge Response")
257 ylabel("Acc  [m/s^2]")
258 xlabel("t  [s]")
259 grid on
260
261 subplot(3,1,2)
262 plot(t_vec,dU)
263 ylabel("Vel  [m/s]")
264 xlabel("t  [s]")
265 grid on
266
267 subplot(3,1,3)
268 plot(t_vec,U)
269 ylabel("Pos  [m]")
270 xlabel("t  [s]")
271 grid on
```

getSolenoid.m

```
function [m_add ,F, m_a, maxAcc, maxVel, range, maxForce] =
    getSolenoid(type, piston_pos, upORdown)
%{
    Returns solenoid force and kinetics and specs.
%}
switch type
    case "SOLENOID_SINGLE"
        m_a = 0.0055;
        m_add = 0.041; % Get more accurate estimate
        range = 0.013;
        % Below, all length units are in mm
        relPos = (piston_pos +range/2)*1000; % Now in millimeter
        maxU_spring = 17.3;
        uSpring = maxU_spring-relPos;
        kSpring = 0.015;
        if upORdown == "up"
            F = -kSpring*uSpring + m_a*9.81;
        elseif upORdown == "down"
            F = 1.72*exp(-0.1771*relPos) + m_a*9.81 - kSpring*
                uSpring;
        else
            F = 0;
        end

    case "SOLENOID_DOUBLE"
        m_a = 0.0055*2;
        m_add = 0.082;
        range = 0.003;
        % Below, all length units are in mm
        relPos_lower = (range/2 + piston_pos)*1000;
        relPos_upper = (range/2 - piston_pos)*1000;
        maxU_spring = 17.3;
        uSpring_upper = maxU_spring-relPos_upper;
        uSpring_lower = maxU_spring-relPos_lower;
        kSpring = 0.015;
        if upORdown == "up"
            F = -1.72*exp(-0.1771*relPos_upper) + kSpring*(
                uSpring_upper-uSpring_lower) + m_a*9.81;
        elseif upORdown == "down"
            F = 1.72*exp(-0.1771*relPos_lower) + kSpring*(
                uSpring_upper-uSpring_lower) + m_a*9.81;
        else
            F = 0;
        end

end
maxAcc = inf;
maxVel = inf;
```

```
45  maxForce = inf;
46  end
```

getActuator.m

```
% actuator types
function [m_tot, m_move, maxAcc, maxVel, range, maxForce] =
    getActuator(type)
%{
    Returns actuator specs.
%}

switch type
    case "NONE"
        range = inf;
        m_move = 0;
        m_tot = 0;
        maxVel = inf;
        maxAcc = inf;
        maxForce = inf;

    case "MICA50CS"
        range = 0.004;
        m_move = 0.15;
        m_tot = 1.2;
        maxVel = inf;
        maxAcc = inf;
        maxForce = 80;

    case "MICA20CS"
        range = 0.001;
        m_move = 0.14;
        m_tot = 0.35;
        maxAcc = 50*9.81;
        maxVel = inf;
        maxForce = 30;

    case "MICA300CM"
        range = 0.012;
        m_move = 0.58;
        m_tot = 3.2;
        maxAcc = 95*9.81;
        maxVel = 1.96;
        maxForce = 540;

    case "LAH13_MINSPEC"
        range = 0.004;
        m_move = 0.00349;
        m_tot = 0.010;
        maxAcc = inf;
        maxVel = inf;
        maxForce = 1.89;

```

```
48      case "LAH13-18-000A-DASH"
49          range = 2*0.00318;
50          m_move = 0.0177;
51          m_tot = 0.127;
52          maxAcc = 879.7;
53          maxVel = inf;
54          maxForce = 15.57;
55
56      case "IDEAL"
57          range = inf;
58          m_move = 0.01;
59          m_tot = 0.01;
60          maxAcc = inf;
61          maxVel = inf;
62          maxForce = inf;
63
64
65
66  end
67
68  end
```

beamData.m

```
1
2  function [L_fn ,b ,h, ro, m] = beamData(fn_wanted, beamType)
3  %{
4      Returns beam spessifications in accordance with the input.
5  %}
6      %% Bridge Dimensions
7      h = 0.008; % meters
8      b = 0.125; % meters
9      I = 1/12 * b*h^3; % meters^4
10
11     %% Material properties for aluminum
12     ro = 2700; % kg/m^3
13     E = 69e9;  % Pa
14
15     %% Derived expression for L(fn)
16     if beamType == "cantiliver"
17         Kn = 3.52;
18     elseif beamType == "doublefixed"
19         Kn = 22.4;
20     end
21     L_fn = (   ( Kn/(2*pi*fn_wanted) )^2 * E*I/(ro*b*h)   )^(1/4);
22
23     %% Calculate Bridge Mass
24     m  = ro*h*b*L_fn;
25
26
27
28
29
30 end
```

regulator.m

```
1 function acc = regulator(a, v, d, Ka, Kv, Kd)
2 %{
3     Returns actuator piston acceleration based on input
4 %}
5 acc = Kd*d + Kv*v + Ka*a;
6 end
```

actuator.m

```
function [F, acc, vel, pos] = actuator(acc_rec, acc_last, vel_last
    , pos_last, dt, type, beamVel, v_thr, p_thr, lastPeriod_max)
%{
Handels actuator responce:
    Calls correct actuator and ensures that the actuator output
    does not exceed the limitation of the actuator in question.
    This functions handels the actions of both solenoid and voice
        coil
    actuators.

NOTE 1: F_try and F is the force from the actuator acting
on the bridge and hence has the opposite sign as the acceleration
of the piston.

NOTE 2: The kinetics of the actuator are always local.
That is, the actuator position, velocity and acceleration is
    relative to
the bridge and not global coordinates.
%}

%% Calculate correct responce
if contains(type,"SOLENOID")
    if lastPeriod_max > p_thr
        if  beamVel > v_thr
            [~, F_sol, m_a,maxAcc, maxVel, range, maxForce] =...
                getSolenoid(type, pos_last, "up");
        elseif beamVel < -v_thr
            [~, F_sol, m_a,maxAcc, maxVel, range, maxForce] =...
                getSolenoid(type, pos_last, "down");
        else
            if vel_last > 0
               [~, F_sol, m_a,maxAcc, maxVel, range, maxForce]
                   =...
                   getSolenoid(type, pos_last, "up");
            else
                [~, F_sol, m_a,maxAcc, maxVel, range, maxForce]
                    =...
                    getSolenoid(type, pos_last, "down");
            end
        end
    else
        [~, F_sol, m_a,maxAcc, maxVel, range, maxForce] =...
                    getSolenoid(type, pos_last, "up");
    end
    acc = -F_sol/m_a;
    vel = vel_last + acc*dt;
    pos = pos_last + vel_last*dt+0.5*acc*dt^2;
    F_try = F_sol;
```

```
44
45 else
46     [~,m_a,maxAcc, maxVel, range, maxForce] = getActuator(type);
47     acc = acc_rec;
48     vel = vel_last + acc*dt;
49     pos = pos_last + vel_last*dt+0.5*acc*dt^2;
50     F_try = -m_a*acc;
51 end
52
53 %% Ensure that actuator does not exeed specs
54 % Force
55 if (abs(F_try) > maxForce)
56     acc = -sign(F_try)*maxForce/m_a;
57     vel = vel_last + acc*dt;
58     pos = pos_last + vel_last*dt+0.5*acc*dt^2;
59 end
60
61 % Acceleration (should be handeled by force and hence never true)
62 if (abs(acc) > maxAcc)
63     acc = sign(acc)*maxAcc;
64     vel = vel_last + acc*dt;
65     pos = pos_last + vel_last*dt+0.5*acc*dt^2;
66 end
67
68 % Velocity
69 if abs(vel) > maxVel
70     acc = 0;
71     vel = vel_last;
72     pos = pos_last + vel_last*dt+0.5*acc*dt^2;
73 end
74
75 % Position
76 if abs(pos) > range/2
77     acc = 0;
78     vel = 0;
79     pos = pos_last;
80 end
81
82 % Calculate force from actuator
83 F = -m_a*acc;
84
85 end
```

newmarkGetResponse.m

```
1  function [u, du, ddu] = Newmark_getResponse(u0, du0, ddu0, dt, m,
       c, k, F)
2  %{
3       Calculates the responce for one time increment using the
4       Newmark Method
5  %}
6
7
8  gamma = 1/2;
9  beta = 1/4;
10
11 ddu = 1/m*(-c*du0 - k*u0 + F);
12
13 du = du0 + (1-gamma)*dt*ddu0 + gamma*dt*ddu;
14
15 ddu_b = (1-2*beta)*ddu0 + 2*beta*ddu;
16
17 u = u0 + dt*du0 + 1/2*dt^2*ddu_b;
18
19 end
```

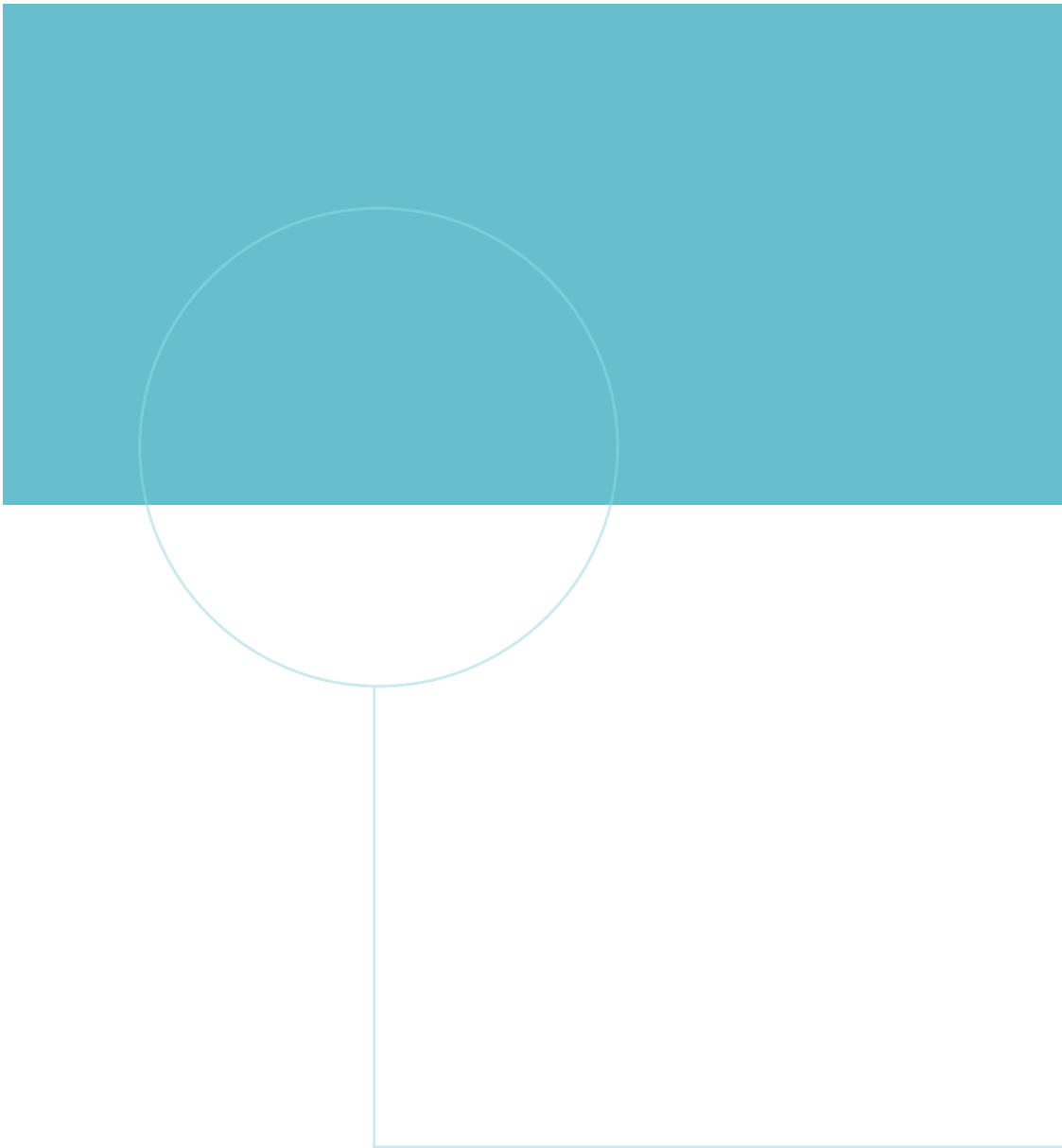

NTNU
Norwegian University of
Science and Technology